KGML-ag: A Modeling Framework of Knowledge-Guided Machine Learning to Simulate Agroecosystems: A Case Study of Estimating N₂O Emission using Data from Mesocosm Experiments

Licheng Liu[1], Shaoming Xu[2], Jinyun Tang[3], Kaiyu Guan[4,5,6], Timothy J. Griffis[7], Matthew D. Erickson[7], Alexander L. Frie[7], Xiaowei Jia[8], Taegon Kim[1, 9], Lee T. Miller[7], Bin Peng[4,5,6], Shaowei Wu[10], Yufeng Yang[1], Wang Zhou[4,5], Vipin Kumar[2], Zhenong Jin[1]*

[1]Department of Bioproducts and Biosystems Engineering, University of Minnesota, Saint Paul, MN, 55108, USA
[2]Department of Computer Science and Engineering, University of Minnesota, Minneapolis, MN, 55455, USA
[3]Climate and Ecosystem Sciences Division, Lawrence Berkeley National Laboratory, Berkeley, CA 94720, USA
[4]Agroecosystem Sustainability Center, Institute for Sustainability, Energy, and Environment, University of Illinois at Urbana-Champaign, Urbana, IL 61801, USA
[5]Department of Natural Resources and Environmental Sciences, University of Illinois at Urbana-Champaign, Urbana, IL 61801, USA
[6]National Center for Supercomputing Applications, University of Illinois at Urbana-Champaign, Urbana, IL 61801, USA
[7]Department of Soil, Water, and Climate, University of Minnesota, Saint Paul, MN 55108, USA
[8]Department of Computer Science, University of Pittsburgh, Pittsburgh, PA, 15260, USA
[9]Department of Smart Farm, Jeonbuk National University, Jeonju, Jeollabuk-do, 54896, Republic of Korea
[10]School of Physics and Astronomy, University of Minnesota, Minneapolis, MN, 55455, USA

Correspondence to: Zhenong Jin (jinzn@umn.edu)

Abstract.

Agricultural nitrous oxide (N₂O) emission accounts for a non-trivial fraction of global greenhouse gases (GHGs) budget. To date, estimating N₂O fluxes from cropland remains a challenging task because the related microbial processes (e.g., nitrification and denitrification) are controlled by complex interactions among climate, soil, plant and human activities. Existing approaches such as process-based (PB) models have well-known limitations due to insufficient representations of the processes or uncertainties of model parameters, and to leverage recent advances in machine learning (ML) a new method is needed to unlock the "black box" to overcome its limitations such as low interpretability, out-of-sample failure and massive data demand. In this study, we developed a first-of-kind knowledge-guided machine learning model for agroecosystems (KGML-ag), by incorporating biogeophysical/chemical domain knowledge from an advanced PB model, *ecosys*, and tested it by comparing simulating daily N₂O fluxes with real observed data from mesocosm experiments. The Gated Recurrent Unit (GRU) was used as the basis to build the model structure. To optimize the model performance, we have investigated a range of ideas, including: 1) Using initial values of intermediate variables (IMVs) instead of time series as model input to reduce data demand; 2) Building hierarchical structures to explicitly estimate IMVs for further N₂O prediction; 3) Using multitask learning to balance the simultaneous training on multiple variables; and 4) Pretraining with millions of synthetic data generated from *ecosys* and fine tuning with mesocosm observations. Six other pure ML models were developed using the same mesocosm data to serve as the benchmark for the KGML-ag model. Results show that KGML-ag did an excellent job in reproducing the mesocosm

N₂O fluxes (overall $r^2 = 0.81$, and RMSE = 3.6 mg N m^{-2} day^{-1} from cross-validation). Importantly KGML-ag always outperforms the PB model and ML models in predicting N₂O fluxes, especially for complex temporal dynamics and emission peaks. Besides, KGML-ag goes beyond the pure ML models by providing more interpretable predictions as well as pinpointing desired new knowledge and data to further empower the current KGML-ag. We believe the KGML-ag development in this study will stimulate a new body of research on interpretable ML for biogeochemistry and other related geoscience processes.

1 Introduction

Nitrous oxide (N₂O), with its global warming potential 273 ± 118 times greater than that of carbon dioxide (CO₂) for a 100-year time horizon, is one of the major greenhouse gases (IPCC6; Forster et al., 2021). The increasing rate of atmospheric N₂O concentration during the period 2010-2015 is 44% higher than during 2000-2005, mainly driven by increased anthropogenic sources that have increased total global N₂O emissions to ~17 Tg N yr^{-1} (Syakila and Kroeze, 2011; Thompson et al., 2019). It is estimated that approximately 60% of the contemporary N₂O emission increases are from agriculture management at global scale (Pachauri et al., 2014; Robertson et al., 2014; Tian et al., 2020), but the estimation uncertainty can exceed 300% (Barton et al., 2015; Solazzo et al., 2021). Quantifying N₂O emissions from agricultural soils is extremely challenging, partly because the related microbial processes, mainly about incomplete denitrification and nitrification, are controlled by many environment and management factors such as temperature/water conditions, soil/crop properties, and N fertilization rate, all of which together have collectively led to large temporal and spatial variabilities of N₂O emissions (Butterbach-Bahl et al., 2013; Grant et al., 2016).

Process-based (PB) models are often used for simulating N₂O fluxes from agroecosystems, but they have some inherent limitations, including incomplete knowledge of the processes, low accuracy due to the under-constrained parameters, expensive computing cost, and rigid structure for further improvements, that we could not resolve by using PB model itself. For example, an advanced agroecosystem model, *ecosys* (Grant et al., 2003, 2006, 2016), simulates N₂O production rates through nitrification and denitrification processes when oxygen (O₂) is limited, with equations considering the influence from related substrate concentrations (e.g., NO₂⁻, N₂O, and CO₂), nitrifier and denitrifier populations, and soil thermal, hydrological physical and chemical conditions. The produced N₂O accumulates, transfers in gaseous phase, aqueous phase, over different soil layers, and eventually exchanges with atmosphere at the soil surface. Other PB models, including DNDC (Zhang et al., 2002; Zhang and Niu, 2016), DAYCENT (Del Grosso et al., 2000; Necpálová et al., 2015), and APSIM (Keating et al., 2003; Holzworth et al., 2014), have also included processes to simulate N₂O production, but adopt different parameterizations using static partition parameters to estimate N₂O emission from nitrification, and other empirical parameters to control the influence on nitrification from soil water content, pH, temperature and substrate concentrations. Besides, N₂O is intimately connected with the soil organic carbon (SOC) dynamics, because soil nitrifiers and denitrifiers interact strongly with aerobic and anaerobic heterotrophs that process SOC evolution, and all of these microbes are driven by shared environmental variables

including soil temperature, moisture, redox status, and physical and chemical properties (Thornley et al., 2007). As expected, these connections make it difficult for PB models, even the most advanced ones like *ecosys*, to find sufficient representations of the physical and biogeochemical processes or obtain enough data to calibrate a large number of model parameters with strong spatio-temporal variations. Thus, novel approaches are needed for addressing the big challenge of agricultural N_2O flux simulations.

Machine learning (ML) models can automatically learn patterns and relationships from data. Recent studies have investigated the potential to predict agricultural N_2O emission with ML models, including random forest (RF, Saha et al., 2021), metamodelling with extreme gradient boosting (XGBoost) (Kim et al., 2021), and deep learning neural network (DNN) (Hamrani et al., 2020). Notably, Hamrani et al. (2020) compared nine widely used ML models for predicting agricultural N_2O. That study pointed out that the long short term memory (LSTM) model with recurrent networks containing memory cells as building blocks will be most suitable for N_2O predictions, but the challenge remains with respect to the ability of capturing the sharp peak of N_2O fluxes and lag time between N fertilizer application and the emission peak. Although there is an increasing interest in leveraging recent advances in machine learning, capturing this opportunity requires going beyond the ML limitations, including limited generalizability to out-of-sample scenarios, demand for massive training data, and low interpretability due to the "black-box" use of ML (Karpatne et al., 2017). PB models with their transparent structures built by representations of physical and biogeochemical processes, seem to be exact complementary to ML models. Thus, combining the power of ML model and PB model understanding innovatively is likely a path forward.

The above need to integrate ML and PB models can be potentially addressed by the newly proposed framework of Knowledge-guided Machine Learning (KGML) models. In the review by Willard et al. (2021), five research frontiers have been identified regarding the development of KGML for diverse disciplines including earth system science, they are: 1) Loss function design according to physical or chemical laws (Jia et al., 2019, 2021; Read et al., 2019); 2) Knowledge-guided initialization through pretraining ML models with synthetic data generated from PB models (Jia et al., 2019, 2021; Read et al., 2019); 3) Architecture design according to causal relations or adding dense layers containing domain knowledge (Khandelwal et al., 2020; Beucler et al., 2019, 2021); 4) Residual modeling with ML models to reduce the bias between PB model outputs and observations (Hanson et al., 2020); and 5) Other hybrid modeling approaches combining PB and ML models (Kraft et al., 2021). These recent advances in KGML pave the pathway to a more efficient, accurate and interpretable solution for estimating N_2O fluxes from the agroecosystem.

In this study, we present a first-of-its-kind attempt of developing a KGML for agricultural GHG fluxes prediction (KGML-ag) with knowledge-guided initialization and architecture design, and demonstrate the potential of KGML-ag with a case study on quantifying N_2O flux observed by a multi-year mesocosm experiments. We designed the KGML-ag structure based on the causal relations of related N_2O processes informed by an advanced agroecosystem model, *ecosys* (Grant et al., 2003, 2006,

2016). We used the synthetic data generated from *ecosys* to design the KGML-ag input/output, and to pre-train the KGML-ag model to learn the basic patterns of each variable. Observations from multi-season controlled-environment mesocosm chambers (Miller, 2021, thesis; Miller et al., 2021, in review) were used to refine the pretrained KGML-ag and evaluate the model performance. Since there is limited literature that guides the development of KGML-ag and not a one that directly addressed GHG fluxes, we investigated a range of ideas to optimize the model performance, including: 1) Using initial values of intermediate variables (IMVs) instead of sequences as model input to reduce data demand; 2) Building hierarchical structures to explicitly estimate IMVs for further N_2O prediction; 3) Using multitask learning to balance the simultaneous training on multiple variables; and 4) Pretraining with millions of synthetic data generated from *ecosys* and fine tuning with mesocosm observations. Although we evaluated the KGML-ag models with real measurements only from a mesocosm experiment, the lessons learned from the development process and various KGML-ag structures can be transferred to other data, other variables and large scale simulations, therefore have broader implications on further KGML related research in agriculture. We believe this study will stimulate a new body of research on interpretable machine learning for biogeochemistry and other related topics in geoscience.

2 Methods

2.1 Experimental design overview

To develop and evaluate the KGML-ag models and compare their performance with pure ML models, we designed the following experiments:

1) With the synthetic data, we developed and pretrained multiple KGML-ag models to learn general patterns and interactions among variables, and evaluated their model performance (Fig. S2, Table 1);

2) With the observed data, we finetuned multiple KGML-ag models to adapt real-world situations, and evaluated their model performance (Fig. 2-3; Fig. S3-5; Table 2-3);

3) We further benchmarked KGML-ag models and uncertainties with other pure ML models without considering temporal dependence, including Decision Tree (DT), Random Forest (RF), Gradient Boosting (GB) from the sklearn package (https://scikit-learn.org/stable/), Extreme Gradient Boosting (XGB) from the XGBoost package (https://xgboost.readthedocs.io/en/latest/) and a 6-linear-layer artificial neural network (ANN) with the mesocosm experiment data by 10 times ensemble experiments (Fig. 4-5; Fig. S6-8);

4) We conducted a few small experiments to further investigate how various model configurations, such as the pretraining process, data augmentation and IMV initial values would influence KGML-ag model performance (Table 3).

2.2 KGML-ag structure development

2.2.1 Generating synthetic data with *ecosys*

We generated synthetic data using a PB model, *ecosys*. The *ecosys* model is an advanced agroecosystem model constructed from detailed biophysical and biogeochemical rules instead of using empirical relations (Grant et al., 2001). It represents N_2O evolution in the microbe-engaged processes of nitrification-denitrification using substrate kinetics that are sensitive to soil nitrogen availability, soil temperature, soil moisture, and soil oxygen status (Grant and Pattey 2008). Two groups of microbial populations, autotrophic nitrifiers and heterotrophic denitrifiers, produce N_2O with specific competitive or cooperative relations in *ecosys* when O_2 availability fails to meet O_2 demand for their respiration, and NO_2^- become alternative electron acceptors. N_2O transfer within soil layers and from soil to the atmosphere is driven by concentration gradient using diffusion-convection-dispersion equations, in the forms of gaseous and aqueous N_2O under control of volatilization-dissolution (Grant et al., 2016). Unlike the pipeline model described by Davidson et al. (2000), which mainly considers the correlations of N_2O production with nitrogen availability and of N_2O emissions with soil water content, *ecosys* enables integrative effects of energy, water, nitrogen availability on N_2O production and N_2O transfer via the microbial population dynamics and their interactions with soil, plant, and atmospheric dynamics, under diverse meteorological and anthropogenic disturbances (e.g. runoff, drainage, tillage, irrigation, soil erosion). Many previous studies have demonstrated its robustness in simulating agricultural carbon and nitrogen cyclings at different spatial/temporal scales, and under different management practices (Grant et al., 2003, 2006, 2016; Metivier et al., 2009; Zhou et al., 2021). For the agricultural ecosystems in the US Midwest, whose simulations are used for synthetic data in this study, the performance of *ecosys* on CO_2 have been extensively benchmarked, including CO_2 exchange (daily Reco R^2 = 0.80-0.86; daily NEE, R^2 = 0.75-0.89) and leaf area index (LAI, R^2 = 0.78) from six flux towers, USDA census reported corn yield (R^2 = 0.83) and soybean yield (R^2 = 0.80), satellite-derived GPP for corn (R^2 = 0.83) and soybean (R^2 = 0.85) in the US Midwest (Zhou et al., 2021). In addition, *ecosys* model can capture the dynamics and magnitude of N_2O flux in hourly frequency (R^2 = 0.2-0.4 and RMSE = 0.1-0.2 mg N m^{-2} h^{-1} in Grant et al., 2008; R^2 = 0.28-0.37 and RMSE = 0.2-0.28 mg N m^{-2} h^{-1} in Grant et al., 2003), and in various ecosystems (e.g. agriculture soil in Grant et al., 2006, 2008; forest in Grant et al., 2010; and grassland in Grant et al., 2016). Therefore, *ecosys* is an appropriate choice of domain knowledge provider and synthetic data generator in the development of KGML models. We generated daily synthetic data including N_2O flux and 76 IMVs (e.g. CO_2 flux from soil, layerwise soil NO_3^- concentration, layerwise soil temperature, and layerwise soil moisture; detailed in Table S1) from *ecosys* simulations for 2000-2018 over 99 randomly selected counties in Iowa, Illinois, and Indiana, USA. We used hourly meteorological inputs (downward shortwave radiation, air temperature, precipitation, relative humidity, and wind speed) from the phase 2 of North American Land Data Assimilation System (NLDAS-2, Xia et al., 2012) and layerwise soil properties (e.g. bulk density, texture, pH, SOC concentration) from the SSURGO database (Soil Survey Staff, 2020) as inputs to *ecosys*. Crop management except N fertilization rates were configured to the same settings as mesocosm experiments (described in Sec 2.2.2). To increase the variability in synthetic data, we

164   implemented 20 different N fertilization rates ranging from 0 to 33.6 g N m^{-2} (i.e. 0 to 300 lb N ac^{-1}) in each simulation of 99

165   counties, and more detailed information for model setup refers to Zhou et al. (2021).

166

167   The generated synthetic data were then processed for further use by KGML-ag development. Meanwhile, the hourly weather

168   forcings were converted to seven daily variables, including the maximum air temperature (TMAX_AIR, ºC), difference

169   between the maximum and the minimum air temperature (TDIF_AIR, ºC), the maximum humidity (HMAX_AIR, fraction),

170   difference between the maximum and the minimum humidity (HDIF_AIR, fraction), surface downward shortwave radiation

171   (RADN, W m^{-2}), precipitation (PREC, mm day^{-1}), and wind speed (WIND, m s^{-1}). Six soil properties were retrieved from the

172   SSURGO database, including total averaged (depth weighted averaged for all layers) bulk density (TBKDS, Mg m^{-3}), sand

173   content (TCSAND, g kg^{-1}), silt content (TCSILT, g kg^{-1}), pH (TPH), cation exchange capacity (TCEC, cmol^{+} kg^{-1}) and soil

174   organic carbon (TSOC, g C kg^{-1}); and two crop properties were retrieved, including planting day of the year (PDOY) and crop

175   type (CROPT, 1 for corn and 0 for soybean). Finally, each synthetic data sample has daily N$_2$O flux, 76 selected IMVs, 7

176   weather forcings (W), 1 N fertilization rate (FN, g N m^{-2}) and 8 soil/crop properties (SCP) (Fig. 1.a; Table S1). The periods

177   from April 1st to July 31st (122 days) were selected to cover the mesocosm observations (around 30 days before and 90 days

178   after N fertilizer date). The total amount of synthetic data sample is 122 days x 18 years x 99 counties x 20 N fertilizer rates

179   (about 4.3 million data points). We randomly selected the samples from 70 counties for training, 10 counties for validation,

180   and 19 counties for testing.

181   **2.2.2 Mesocosm experiments for KGML-ag model fine-tuning and evaluation**

182   Observations were acquired from a controlled-environment mesocosm facility on the St. Paul campus of the University of

183   Minnesota. Soil samples were sourced in 2015 from a farm in Goodhue County, MN (44.2339º N and 92.8976º W), which had

184   been under corn-soybean rotation for 25 years. Six chambers with a soil surface area of 2 m^2 and column depth of 1.1 m were

185   used to plant continuous corn during 2015-2018 and monitor the N$_2$O flux response to different precipitation treatments. The

186   experiment also measured other environmental variables including air temperature and photosynthetically active radiation

187   (PAR), which were controlled to mimic the outdoor ambient environment. Granular urea fertilizer was hand broadcasted and

188   incorporated to a depth of 0.05 m to each chamber at a rate of 22.4 g N m^{-2} (200 lb N ac^{-1}) on May 1st of 2015, May 4th of

189   2016 and May 3rd of 2017, and 10.3 g N m^{-2} (92 lb N ac^{-1}) on May 8th of 2018. Corn hybrid (DKC-53-56RIB) were hand

190   planted to a depth of 0.05 m in two rows spaced 0.76 m apart 3-5 days after fertilizer application, at a seeding rate of 35,000

191   seeds ac^{-1} in 2015 to 2017, and 70,000 seeds ac^{-1} in 2018 but thinned upon emergence to ensure 100 percent emergence at

192   35,000 seeds ac^{-1}. Crops were harvested at the end of September by cutting the stover five inches above the soil. Hourly N$_2$O

193   fluxes (mg N m^{-2} h^{-1}) and CO$_2$ fluxes (g C m^{-2} h^{-1}) were measured using non-steady-state flux chambers with a CO$_2$ analyzer

194   (LI-10820 for 2016 and LI-7000 for 2017 and 2018, LI-COR Biosciences, Lincoln, NE) and a N$_2$O analyzer (Teledyne

195   M320EU, Teledyne Technologies International Corp, Thousand Oaks, CA) (Detail method can be retrieved from Fassbinder

196   et al., 2012, 2013). We also collected soil moisture at 15 cm depth (VWC as abbreviation of volumetric water content, m^3 m$^-$

197 [3]), weekly 0-15 cm depth soil $NO_3^- + NO_2^-$ concentration (NO_3^- for short in the following text, g N Mg^{-1}), soil NH_4^+

198 concentration (NH_4^+, g N Mg^{-1}), and related environment variables including air temperature, radiation, humidity and soil/crop

199 properties from three growing seasons during 2016-2018 and six mesocosm chambers (Fig. S1). The magnitude of N_2O flux

200 and NO_3^- soil concentration and their responses following fertilizer application from this mesocosm experiment are slightly

201 higher than several field studies of agricultural soils (Fassbinder et al., 2013; Grant et al., 1999, 2006, 2008, 2016; Hamrani et

202 al., 2020; Venterea et al., 2011). More details about the mesocosm facility and experimental design can be found in the thesis

203 of Miller L. (2021).

204

205 The observed data were then processed to fine-tune and evaluate the KGML-ag models. The N_2O flux and four IMVs and

206 weather variables were collected from the measurements in the selected period (i.e., April 1st to July 31st). Weekly NO_3^- (short

207 for soil NO_3^- within 0-15 cm depth), and NH_4^+ (short for soil NH_4^+ within 0-15 cm) were linearly interpolated to the daily time

208 scale on days containing VWC (short for soil VWC in 15 cm) data. Hourly air temperature, net radiation, N_2O (short for N_2O

209 fluxes from soil), CO_2 (short for CO_2 fluxes from soil) and VWC were resampled to daily scale. All SCP were derived from

210 mesocosm measurements except that TCEC was derived from the SSURGO database according to the soil origin. We used the

211 leave-one-out cross-validation (LOOCV) method for the evaluation process. Each time we used five chambers' data for model

212 finetuning and another one chamber data for validation. For example, if we used chamber 1-5 to train the model, then chamber

213 6 would serve as the out-of-sample data to validate the results. Only the validation results would be presented in our study.

214

215 To reduce overfitting and increase the generalization of the trained model based on the small amount of mesocosm data, we

216 applied the following method to augment the experimental measurements and weather forcings to 1000 times larger by

217 sampling hourly data and averaging them to daily scale. In this method, 16 hours (or maximum valid hours) of data are

218 randomly selected from 24 hours of data to compute their mean as the daily value. Since up to 2/3 of the day is covered by the

219 selected data (16 hours /24 hours), the augmented daily values should be representative enough for the source day with slight

220 variations from each other. Furthermore, the observation ratio, (24 hours - missing hours) / 24 hours, can be used as the weights

221 in loss function to inject the data quality information in model optimization. If the day has more than 16 hours missing values,

222 we consider the observations in that day as not trustworthy and drop the day by setting the weight to 0. This method can not

223 only augment the data to 1000 times larger but also deal with the missing values in observed data inherently. The total amount

224 of observed mesocosm data and related weather forcings are augmented to 122 days x 3 years x 6 chambers x 1000 data

225 samples in this study.

226

227 **2.2.3 Gated Recurrent Unit (GRU) as the basis of KGML-ag**

228 Hamrani et al. (2020) compared different models and reported that LSTM provided the highest accuracy in predicting N_2O

229 fluxes, because N_2O flux is time dependent by its production/consumption nature and LSTM simulates target variables by

considering both current and historical states. The LSTM model, proposed by Hochreiter and Schmidhuber (1997), uses a cell state as an internal memory to preserve the historical information. At each time step, it creates a set of gating variables to filter the input and historical information and then uses the processed data to update the cell state. Similar to LSTM, GRU is a gated recurrent neural network but only keeps one hidden state (Cho et al., 2014). Though simpler than LSTM, GRU is proved to have similar performance (Chung et al., 2014). Our preliminary test on synthetic data for N_2O prediction showed that GRU indeed provided similar or higher accuracy and model efficiency under different model settings than LSTM (Table S2). This is possible because simpler models with fewer weights and hyperparameters are more robust in combating the overfitting problem. Therefore, we choose GRU as the basis of KGML-ag development.

2.2.4 Incorporating domain knowledge to the development of KGML-ag

To quantitatively reveal the correlations between N_2O fluxes and IMVs and guide the KGML-ag development, we conducted feature importance analysis by a customized 4-layer GRU ML model (Fig. 1b). Each layer of the model has a GRU cell with 64 hidden units. The 4-layer structure makes the model deeper and capable of capturing complex interactions. Between each GRU cell, 20% of the output hidden states are randomly dropped by replacing them with zero values (so called 20% dropout) to avoid overfitting. A linear dense layer is used to map the final output to N_2O. We first trained GRU models using synthetic data with different combinations of IMVs as inputs to predict the N_2O fluxes (original-test, Table S2). The feature importance analysis of well-trained models was then implemented by replacing one input feature with a Gaussian noise with mean $\mu=0$ and standard deviation $\sigma=0.01$, while keeping others untouched (new-test). The importance score was calculated by the new-test's root mean square error (RMSE) (replacing one feature) minus the original-test's RMSE (no replacing). RMSE was calculated by $\frac{\sqrt{\Sigma_1^N(y_i - y_i')^2}}{N}$ where N is the total number of observations across time and space, y_i is i-th measurement from synthetic data or observed data and y_i' is its corresponding prediction.

To find important variables for N_2O flux prediction in an ideal situation where all variables are available, we conducted a feature importance analysis for GRU models with all IMVs and basic inputs including FN, 7 W and 8 SCP (Fig. S2a). Results indicated that flux variables including NH_3, H_2, N_2, O_2, CH_4, evapotranspiration (ET) and CO_2 had significant influence on the model performance. Variables ranked high in feature importance analysis are considered with priority during model development. To develop a functionable KGML-ag, we further investigated the feature importance of four IMVs that are available from mesocosm observations including CO_2, NO_3^-, VWC and NH_4^+, which were ranked 7th, 20th, 58th, 60th respectively in 92 input features of synthetic data (Fig. S2a). We used these four available IMVs to create two input combinations: 1) CO_2 flux, NO_3^-, VWC and NH_4^+ (IMVcb1), and 2) NO_3^-, VWC and NH_4^+ (IMVcb2). The objective of building IMVcb2 was to investigate the importance of the highly ranked variable CO_2 flux (by removing it from the inputs), and the impact of mixing-up flux and non-flux variables on model performance. We tested the feature importance of the GRU models built with IMVcb1 and IMVcb2 to check whether they would help in N_2O prediction (Fig. S2b-c). All the feature

importance results above indicated the correlation intensity between N_2O and many other variables, which would help the KGML-ag model development and interpretation in this study (rest of this section and Sec. 3.1), and would guide future N_2O related measurements and KGML model development (discussed in Sec. 4.3).

Next we used the knowledge learned from synthetic data to develop the structure of KGML-ag (Fig. 1c-d). Previous studies for KGML models have used physical laws, e.g., conservation of mass or energy, to design the loss function for constraining the ML model to produce physically consistent results (Read et al., 2019; Khandelwal et al., 2020). However, for complex systems like agroecosystems, it is challenging to incorporate physical laws, such as mass balance for N_2O, into the loss function due to the incomplete understanding of the processes and the lack of mass balance related data for validation. An alternative solution is to incorporate such information in the design of the neural network (Willard et al., 2021). Effectiveness of such an approach was demonstrated by Khandelwal et al. (2020) in the context of modeling stream flow in a river basin using Soil & Water Assessment Tool (SWAT). They used a hierarchical neural network to explicitly model IMVs (e.g., soil moisture, snow cover) and their relationships with the target variable (streamflow) and showed that this model is much more effective than a neural network that attempts to directly learn the relationship between input drivers and the target variables. Following this idea, we identified four desired features of an effective KGML-ag model, including: 1) We used initial values instead of sequence of the IMVs from synthetic data or observed data to provide a solid starting state for the ML system and reduce the IMV data demand, and then used the rest of the data to further constrain the prediction of IMVs; 2) We built a hierarchical structure based on the structure of process representation in *ecosys* to first predict IMVs and then simulate N_2O with predicted IMVs; 3) We trained all variables together using multitask learning to reach the best prediction scores, which generalized the model and incorporated interactions between IMVs and N_2O; 4) We initialized the KGML-ag model by pretraining with synthetic data before using real observed data to transfer physical knowledge, which further reduced the demand on large training samples and aided in faster convergence for fine-tuning.

To meet these desired features, we proposed two KGML-ag models (Fig. 1c-d). The first model, KGML-ag1, is a hierarchical structure containing two modules to simulate IMVs and N_2O sequentially. Each module is a 2-layer 64 units GRU ML model. The inputs to the module of the KGML-ag1 model for IMV predictions (KGML-ag1-IMV module) are FN, 7W and 8SCP together with the initial values of IMVs, and the outputs are IMV predictions. The inputs to the module of the KGML-ag1 model for N_2O predictions (KGML-ag1-N_2O module) are FN, 7W, 8SCP and predicted IMVs from KGML-ag1-IMV, and the output is the target variable N_2O. Linear dense layers were coded for both modules to map output states to IMVs or N_2O. The dropout method was applied to drop 20% of the state output between GRU cells and dense layers. The second model, KGML-ag2, is also a hierarchical structure similar to KGML-ag1, but has multiple KGML-ag2-IMV modules to explicitly simulate IMVs by tuning them separately in the fine-tuning process (discussed in Sec. 2.2.5). Each KGML-ag2-IMV module in KGML-ag2 is a 2-layer 64 units GRU cell with the inputs of FN+7W+8SCP and one IMV initial value, and the output of one IMV

295 prediction. The KGML-ag2-N$_2$O module collects the IMV predictions from KGML-ag2-IMV modules and predicts the N$_2$O

296 with inputs of FN+7W+8SCP and predicted IMVs.

2.2.5 Strategies for pretraining and fine-tuning processes

298 To increase the efficiency of the training process, we used the Z-normalization ($\frac{(X-\mu)}{\sigma}$, where X is the vector of a particular

299 variable over all the data samples in the data set; μ is the mean value of X; σ is the standard deviation of X) method to

300 normalize each variable separately on synthetic data. Then the scaling factors (μ, σ) derived from *ecosys* synthetic data for

301 each variable were used to Z-normalize observed data into the same ranges as synthetic data. As mentioned in Sec. 2.2.1, the

302 TDIF_AIR, HDIF_AIR were used instead of absolute min temperature (TMIN_AIR) and humidity (HMIN_AIR). This is done

303 because TMIN_AIR and HMIN_AIR follow similar trends as TMAX_AIR and HMAX_AIR, making Z-normalization

304 numerically poorly defined. Using the difference between maximum and minimum can provide a clearer information of daily

305 air temperature/humidity variation.

306

307 During the pretraining process, we initialized the IMV of KGML-ag using the first day value of synthetic IMV time series.

308 Adam optimizer with a start learning rate of 0.0001 was used for the training process. The learning rate would decay by 0.5

309 times after every 600 training epochs. At each epoch, synthetic data samples were randomly shuffled before being input to the

310 model to predict N$_2$O (and IMVs if any). The mean square error (MSE) loss (calculation was equal to the square of RMSE) or

311 sum of MSE loss (if multitask learning) between predictions and *ecosys* synthetic observations were calculated to optimize the

312 weights of GRU cells. After the training process updated the model's weights, the validation process was performed to evaluate

313 the model performance based on untouched samples with RMSE and the square of Pearson correlation coefficient (r^2). r^2 was

314 calculated as $\frac{\left(\sum_i (y_i' - \underline{y_i'})(y_i - \underline{y_i})\right)^2}{\sum_i (y_i' - \underline{y_i'})^2 (y_i - \underline{y_i})^2}$, where y_i is the i-th measurement from synthetic data or observed data, y_i' is its

315 corresponding prediction, $\underline{y_i}$ is the mean of the measurement y in diagnosing space and $\underline{y_i'}$ is the mean of the predicted y' in

316 diagnosing space. If both validated r^2 and RMSE were better than the best values in previous epochs, the updated model in this

317 epoch would be saved. Normalized RMSE (NRMSE, calculated by RMSE/(max-min) of each variable observation) was

318 introduced to evaluate IMV predictions between variables with different value ranges.

319

320 During the fine-tuning process, we used estimated IMV initial values of 1.0 g C m^{-2}, 0.2 m^3 m^{-3}, 0.0 g N Mg^{-1}, and 20.0 g N

321 Mg^{-1} for CO$_2$, VWC, NH$_4^+$, and NO$_3^-$ respectively, from starting day (April 1st) to the day before the first day of real

322 observations, as input to KGML-ag models. Then the first-day values of observed IMVs were input into KGML-ag during the

323 rest days of the period as IMV initial values. In addition, as described in Sec. 2.2.2, we used a data augmentation method to

324 augment the total amount of data 1000 times larger for the fine-tuning process. The purpose of this data augmentation method

325 was to increase the generalization of the fine-tuned model and to overcome the overfitting due to small sample size. The mask

matrix was elementarily multiplied to the output matrix to calculate the MSE, r^2 and RMSE only for days with observations. The similar optimizer was used with an initial learning rate of 0.00005 and decay fraction of 0.5 per 200 epochs. Other training/validation methods in each epoch were similar to the pretraining process. Specifically, in the KGML-ag1 model finetuning process, we first froze the KGML-ag1-N$_2$O module and only trained the KGML-ag1-IMV module for IMVs. After finishing the KGML-ag1-IMV module training, we froze the KGML-ag1-IMV module and trained the KGML-ag1-N$_2$O module for N$_2$O. In the KGML-ag2 fine-tuning process, the similar freezing method was used but different KGML-ag2-IMV modules were trained separately one by one.

2.3 Development environment description

We used the Pytorch 1.6.0 (https://pytorch.org/get-started/previous-versions/) and python 3.7.9 (https://www.python.org/downloads/release/python-379/) as the programing environment for the model development. In order to use the GPU to speed-up the training process, we installed cudatoolkit 10.2.89 (https://developer.nvidia.com/cuda-toolkit). A desktop with Nvidia 2080 super GPU was used for code development and testing. The Mangi cluster (https://www.msi.umn.edu/mangi) from High Performance Computing of Minnesota Supercomputing Institute (HPC-MSI, https://www.msi.umn.edu/content/hpc) with 2-way Nvidia Tesla V100 GPU was used in training processes which consumed longer time and bigger memories.

3 Results

3.1 Pretraining experiments using synthetic data from *ecosys*

In the pretraining stage, the GRU model with 76 IMVs achieved the best performance in predicting N$_2$O fluxes (r^2=0.98, RMSE =0.54 mg N m^{-2} day^{-1} and normalized RMSE (NRMSE) = 0.01) on the test set of synthetic data generated from *ecosys* (Table 1). The high performance was due to some flux IMVs such as NH$_3$, H$_2$, O$_2$, CO$_2$ and ET, which are highly correlated to N$_2$O (Fig. S2a), were used as input to the model. The good performance of GRU with all IMVs indicates that ML models are able to perfectly mimic *ecosys* when sufficient information about IMVs is available. The GRU model with only basic input of N fertilizer rate, 7 weather forcings, and 8 soil/crop properties (FN+7W+8SCP) had the accuracy of r^2=0.89 and RMSE = 1.37 mg N m^{-2} day^{-1} (Table 1). The relatively low performance is likely because this model failed to capture several highly nonlinear pathways that are employed by ecosys to predict N$_2$O (e.g., one influence pathway from precipitation to N$_2$O can be: Precipitation → soil moisture → N components solubility/concentration → nitrification/denitrification rate/amount → soil N$_2$O concentration → gas N$_2$O flux). When adding sequences of IMV combinations (i.e., IMVcb1 of CO$_2$ flux, NO$_3^-$, NH$_4^+$ and VWC, and IMVcb2 of NO$_3^-$, NH$_4^+$ and VWC), the GRU models performed slightly better than the GRU model using only basic inputs, achieving r^2 of 0.92 and 0.90, respectively (Table 1). The KGML-ag1 with IMVcb1 and IMVcb2 initial values provided better performance (both r^2 = 0.90) than GRU with basic input and comparable performance to the GRU with inputs

of IMVcb1 and IMVcb2 sequence. Besides, KGML-ag1 provided predicted IMVs of CO_2, NO_3^-, NH_4^+, and VWC with r^2 over 0.91, and NRMSE below 0.06 (Table 1). KGML-ag2 also provided comparable N_2O performance but relatively better IMVs performance of r^2 over 0.92 and NRMSE below 0.05. Results indicated that KGML-ag models with IMV initial values as extra input performed similar or better than pure ML models in synthetic data.

3.2 KGML-ag evaluation using observed data from mesocosm

After being fine-tuned with observed data, KGML-ag1 had N_2O prediction overall accuracy of r^2=0.81 and RMSE=3.6 mg N m^{-2} day^{-1}, while non-pretrained GRU model provided r^2=0.78 and RMSE=4.0 mg N m^{-2} day^{-1}, and pretrained GRU model provided r^2=0.80 and RMSE=3.77 mg N m^{-2} day^{-1} (Table 3). The time series of N_2O predictions from KGML-ag1 and the non-pretrained GRU model were further compared (Fig. 2), from which we found at least two advantages of using KGML-ag1 for N_2O predictions: 1) For the region without observation data (normally before day 25), KGML-ag1 predicted stable N_2O fluxes close to 0 mg N m^{-2} day^{-1} (which is close to the reality in the experiment setting) while GRU caused anomalous peaks of fluxes. This is because KGML-ag1 has learned knowledge for the whole period from the pretraining process with *ecosys* model generated synthetic data, but GRU model has no prior knowledge for the period without any data in observations; 2) Although KGML-ag1 had a lower accuracy than GRU in some chambers, KGML-ag1 can better capture the temporal dynamics of N_2O fluxes compare to GRU, especially when the fluxes are highly variable (e.g. Fig 2 chamber 2).

To validate KGML-ag1 robustness, we further investigated the KGML-ag1 and GRU model performance in different temporal windows, shrinking from the whole period to the N_2O peak occurrence time (days 1-122, day 30-80, day 40-65 and day 45-60 for year 2016-2018), and performance in N_2O flux, first order gradient of N_2O (slope) and second order gradient of the N_2O (curvature) (Table 2). Slope represents the speed of N_2O flux changes through time and curvature represents the acceleration. Assessing prediction performance with these two metrics will reveal the model robustness on capture variable dynamics, which is critical when predicting fast-change variables with hot moments (a short period of time with rare events like flux increasing quickly) like N_2O. First of all, the overall r^2 and RMSE of KGML-ag1 for values, slope and curvature were always better than GRU. In particular, KGML-ag1 captured the peak region (e.g., days 45-60) much better than GRU in both magnitude and dynamics (Table 2, Fig 2). Even for chamber 2 and 5 in which KGML-ag1 made worse N_2O predictions than GRU (Δr^2 ranging from -0.07 to -0.03), it better captured temporal dynamics than GRU in terms of slope (Δr^2 ranging from 0.08 to 0.16) and curvature (Δr^2 from 011 to 0.23) (Table 2). For other chambers, KGML-ag1 outperformed GRU consistently. For chamber 1, KGML-ag1 had worse N_2O predictions RMSE than GRU but the Δr^2 increased as the window shrinks to the peak emission time (0.07 → 0.13). The slope and curvature for chamber 1 also indicated that KGML-ag1 captured the dynamics much better than GRU. For chamber 3, KGML-ag1 predicted better N_2O but presented worse slope and curvature RMSE than GRU (Table 2). However, when explicitly investigating the time series of N_2O flux, slope and curvature in each year, KGML-ag1 outperformed GRU more significantly in 2017, the year with more complex temporal dynamics of N_2O fluxes, than in 2016

388 and 2018, especially for chamber 3 (Fig. 2; Fig. S3-4). This investigation supported that KGML-ag1 was more capable for

389 complex dynamics predictions.

390

391 Interestingly, the fine-tuned KGML-ag1 model predicted reasonable IMVs including CO_2, NO_3^-, NH_4^+, and VWC with overall

392 r^2 of 0.37, 0.39, 0.60, and 0.33 and NRMSE of 0.14, 0.21, 0.09 and 0.18, respectively (Table 3). The time series comparisons

393 between IMV predictions and observations further indicated that KGML-ag1 could reasonably capture both magnitude and

394 dynamics (Fig. 3). KGML-ag2 presented better IMVs predictions than KGML-ag1, with overall r^2 of CO_2, NO_3^-, NH_4^+, and

395 VWC increasing by 0.37, 0.17, 0.06 and 0.51, and NRMSE decreasing by 0.05, 0.03, 0.01 and 0.10, respectively, but a slightly

396 lower r^2 (decreasing 0.02) of N_2O (Table 3; Fig. S5). This indicated that explicitly simulating each IMV with separated KGML-

397 ag2-IMV modules did not benefit the N_2O flux prediction accuracy, likely due to increasing model complexity which resulted

398 in reduced stability and ignoring the IMV interactions. In addition, we also found all KGML-ag models would perform better

399 by using IMVcb1 (with CO_2) than using IMVcb2 (without CO_2) in real data tests, indicating feature importance analysis based

400 on synthetic data can be a reasonable substitute for analysis with the often limited real-world data.

401 **3.3 KGML-ag comparing with other pure ML models**

402 The results from eight different models showed that KGML-ag1 comparing with other pure ML models consistently provided

403 the lowest RMSE (3.59-3.94 mg N m^{-2} day^{-1}, 1.14-1.23 mg N m^{-2} day^{-2}, and 0.84-0.89 mg N m^{-2} day^{-3}) and highest r^2 (0.78-

404 0.81, 0.48-0.56, and 0.23-0.31) for N_2O fluxes, slope and curvature, respectively (Fig. 4). This indicated that KGML-ag1

405 outperformed other pure ML models in capturing both the magnitude and dynamics of N_2O flux. Meanwhile, we have

406 calculated the uncertainty of mesocosm measurement due to converting hourly data to daily data during 30-80 days by using

407 augmented values minus the mean of the augmented values with lower and upper limits being -10.2 and 10.4 mg N m^{-2} day^{-1},

408 respectively (-10.2 to 10.4 mg N m^{-2} day^{-1}, and standard deviation =1.4 mg N m^{-2} day^{-1}). KGML-ag1 during the same period

409 has comparable uncertainties based on ensemble simulations with lower and upper limits being -14.4 and 15.2 mg N m^{-2} day^{-1}

410 $^{-1}$, respectively (calculated by ensemble values minus the mean of ensemble values; -14.4 to 15.2 mg N m^{-2} day^{-1}, with standard

411 deviation = 1.3 mg N m^{-2} day^{-1}). KGML-ag2 presented slightly better mean scores for N_2O flux predictions than KGML-ag1,

412 but worse scores for slope and curvature and larger uncertainties. This proved the hypothesis discussed in section 3.2 that

413 KGML-ag2 didn't benefit the magnitude and dynamics predictions of N_2O flux with its more complex structure and less

414 connections between IMVs.

415

416 Within the tree-based models (DT, RF, GB and XGB), the simplest model DT provided the worst predictions for N_2O flux,

417 slope and curvature. The XGB model provided the highest N_2O flux accuracy with r^2 of 0.61-0.63 and RMSE of 5.07-5.17 mg

418 N m^{-2} day^{-1}, while the GB model provided best slope and curvature predictions with r^2 of 0.38-0.40 and 0.23-0.26, and RMSE

419 of 1.34-1.37 mg N m^{-2} day^{-2} and 0.91-0.95 mg N m^{-2} day^{-3}, respectively. The highest N_2O flux accuracy and relatively low

420 slope and curvature accuracy of the XGB model implied that there is a trade-off between the abilities of capturing dynamics

421 and magnitude.

422

423 In the group of deep learning models including ANN, GRU and KGML-ag1, ANN provided the worst predictions. Even with

424 the better N_2O flux predictions than most tree-based models (except XGB), the slope and curvature predictions of ANN were

425 the worst among all eight models. This implied that the trade-off between accurately capturing N_2O dynamics to magnitude in

426 ANN was significant. But when considering the temporal dependence, deep learning model GRU and KGML-ag1

427 outperformed all other models in flux, slope and curvature predictions. This indicated that without considering temporal

428 dependence the improvement in N_2O flux prediction accuracy could be risky by causing the performance drop in capturing

429 dynamics.

430

431 The detailed model comparisons in each chamber are shown in Fig. 5 (N_2O flux) and Fig. S6-7 (N_2O slope and curvature),

432 where the results are found to follow the same pattern as described above. In addition, time series comparisons of chamber 3

433 and 4 in 2017 between different models are presented in Fig. S8 as two examples. For periods without any observed data, we

434 assumed that the good model predictions should be stable, consistent with the nearest period and close to the reality in the

435 experiment setting (e.g. no erratic peak and N_2O flux near 0 mg N m^{-2} day^{-1} before day 25). From these comparisons, we infer

436 that without considering temporal dependence and pretraining process, the tree-based model including DT, RF, GB and XGB

437 and deep learning model ANN predicted erratic peaks in almost every missing data point, while the GRU model was stable in

438 short missing period (1-2 days of missing data) and only presented poor performance in long missing period (before day 25).

439 This improvement by the GRU model may be attributed to the structure of GRU that naturally keeps the historical information

440 using hidden states, which enables GRU to consider the temporal dependence and make consistent predictions over time.

441 **3.4 Influence of pretraining process, data augmentation and using IMV initial values as input feature**

442 After we pretrained the GRU model with synthetic data, the overall r^2 of N_2O flux predictions in observed data increased by

443 0.02, 0.12 and 0.14, and RMSE decreased by 0.23 mg N m^{-2} day^{-1}, 0.15 mg N m^{-2} day^{-2} and 0.02 mg N m^{-2} day^{-3} for flux, slope

444 and curvature predictions, respectively, compared to non-pretrained GRU (No.1-6 in Table 3). The gap between the GRU

445 model with pretrain and KGML-ag1 in N_2O value prediction shows the improvement resulting from architecture change (r^2

446 increases by 0.01 and RMSE decreases by 0.17 mg N m^{-2} day^{-1}). Although pretrained GRU had higher slope and curvature

447 prediction accuracy than KGML-ag models, it still couldn't achieve the current N_2O value prediction accuracy of KGML-ag1.

448 Besides, the KGML-ag models had relatively shallow N_2O prediction modules (2-layer GRU KGML-ag-N_2O module of

449 KGML-ag models vs 4-layer GRU) but included modules for IMV predictions, which therefore increased the model

450 interpretability.

451

452 It's worth noting that prediction accuracy of all KGML-ag models dropped without augmenting the training dataset in the fine-

453 tuning process (No.7-10 in Table 3). Moreover, the maximum training epochs increased from 800 to 20000, which resulted in

454 overfitting on the small data set. This indicated that the data augmentation indeed helped the models become more

455 generalizable and gain better accuracy.

456

457 Experiments using zero initial values presented a significant drop in every variable's prediction accuracy (No.11-14 in Table

458 3). This indicated that the IMV initial values input into the KGML-ag-IMV modules of KGML-ag models influenced not only

459 the IMV prediction but also the N_2O prediction of the KGML-ag-N_2O module. This shows that there is useful information

460 transferred from IMVs in the KGML-ag-IMV module to the KGML-ag-N_2O module.

461 **4 Discussion**

462 In the previous section, we showed that KGML-ag models can outperform ML models, by invoking architectural constraints

463 and PB model synthetic data initialization. Compared to traditional PB models such as *ecosys*, KGML-ag models provide

464 computationally more accurate and efficient predictions (KGML-ag few seconds vs *ecosys* half hour), which is similar to

465 traditional ML surrogate models (Fig. S9). But KGML-ag goes beyond that by providing more interpretable predictions than

466 pure ML models.

467 **4.1 Interpretability of KGML-ag**

468 The proposed KGML-ag models incorporate causal relations among N_2O related variables/processes as shown in Fig. S10.

469 Managements, weather forcings and initial values of IMVs influence soil water, soil temperature and soil properties, which

470 influence the availability of O_2 and N as well as the microbe populations in soil, and further influence the nitrification and

471 denitrification rates. N_2O is produced during both nitrification and denitrification when soil O_2 concentration is limited. Our

472 KGML-ag follows this hierarchical structure by designing KGML-ag-IMV modules representing the soil processes for IMVs

473 predictions (Fig. 1c-d).

474

475 To better explain the time series predictions of N_2O flux (Fig. S1; Fig. 2-3), we separated the observations of each year into

476 three periods: leading period (before N_2O increasing), increasing period (increasing to the peak) and decreasing period (peak

477 decreasing to near zero). During the leading period, both NH_4^+ and CO_2 were increasing immediately in the following few days

478 following urea N fertilizer application, indicating that urea was decomposing into NH_4^+ and CO_2 in soil water. With

479 accumulating NH_4^+ in soil, nitrification started producing NO_3^- and consuming O_2. N_2O didn't respond to the fertilizer

480 immediately due to enough O_2 in soil. Then when the soil became sufficiently hypoxic, N_2O fluxes entered an increasing

481 period with N_2O being produced by nitrification and denitrification processes. CO_2 fluxes were relatively low and NH_4^+ kept

482 decreasing during this period. Finally, when soil NH_4^+ was exhausted and NO_3^- started decreasing due to denitrification, N_2O

483 fluxes then entered the decreasing period. CO_2 flux was related to urea decomposition during the leading period, and was more
484 closely related to O_2 demand in other periods. The KGML-ag predictions of N_2O and IMV captured the three periods and
485 transition points, demonstrating the connections between those variables following the description as above (Fig. 3; Fig. S5).
486 Although KGML-ag1 obtained lower IMVs prediction accuracy compared to KGML-ag2, it captured the general trends and
487 was doing better for transitions, especially in NH_4^+ predictions. KGML-ag2 overfitted on the observations and ignored the
488 correlations between IMVs, which resulted in loss in pretrain knowledge, poorer performance in the leading period, and erratic
489 predictions in the period with missing observations (before day 25).

490 **4.2 Lessons for KGML-ag development**

491 The development of KGML-ag in our study is suitable to predict not only N_2O but also other variables, such as CO_2, CH_4 and
492 ET, with complicated generation processes relying on the historical states. To develop a capable KGML model, we need to
493 carefully address three questions:

494

495 What kind of ML model is suitable for developing KGML? The answer could be determined by the dominant variation type
496 of the target variable in the data. If the dominant type is temporal variance, like flux variables in high temporal resolution (e.g.,
497 daily, or hourly), we should consider ML models with temporal dependency. RNN models such as GRU used in this study,
498 and CNN models such as casual CNN (Oord et al., 2016) can be good starting ML models. If the dominant type is spatial
499 variation, like variables in coarse temporal resolution (e.g., monthly or annually) but with high diversity due to soil property,
500 land cover and climate, we should consider ML models with the ability to deal with edges, hotpoints and categories, such as
501 CNN;

502

503 What physical/chemical constraints can be used to build KGML models? Although physical rules such as mass balance or
504 energy balance are conceptually straightforward and were proved capable of constraining KGML in predicting lake phosphorus
505 and temperature dynamics (Hanson et al., 2020; Read et al., 2019), they were excluded in this study according to our
506 preliminary analysis. The reason is that the mass balance equation of N in the agriculture ecosystem includes too many
507 unknown and unobservable components such as N_2 flux, NH_3 flux, N leaching, microbial N, plant N and soil/plant exchange,
508 which collectively introduce large uncertainties in balance equations and make them hard to be directly applied in the KGML-
509 ag framework. Other related physical (e.g., diffusion, solution) or chemical (e.g., nitrification, denitrification) processes cannot
510 be easily added into the KGML-ag structure as rules due to lack of understanding of the process. Instead, as mentioned in Sect.
511 2.2.4, we used hierarchical structure to enforce an architectural constraint and causal relations among variables, and pretraining
512 processes to infuse knowledge from *ecosys* to KGML-ag models.

513

514 How to involve PB models in the KGML development? An advanced PB model like *ecosys* built upon biophysical and
515 biochemical rules instead of empirical relations will be a good basis to learn the process, guide the structure and provide the

516 constraints for KGML. The generated synthetic data in this study helped us get some knowledge about variables such as their
517 general trends, dynamics and correlations. Such knowledge can be transferred to KGML models from synthetic data in the
518 pretraining process, which can reduce the efforts to collect large numbers of real-world observation data. Moreover, while
519 KGML shows great potential beyond PB models, we reckon that equally important for improving N_2O modeling is to continue
520 improving our understanding of the related processes and mechanisms. Novel data collection and incorporating new
521 understanding into PB models (e.g., *ecosys*) could provide foundation to further empower KGML (see further discussion in
522 Sect. 4.3).

523

524 4.3 Limitation and possible improvement

525 First, the KGML-ag models in this study are limited by the available observed data. The mesocosm measurements of N_2O
526 fluxes (16.9 ± 11.7 mg N m^{-2} day^{-1} during days of 45-60; Highest value is 71 mg N m^{-2} day^{-1}) and NO_3^- soil concentrations
527 (59.3 ± 20.7 g N Mg^{-1} during days of 45-60; Highest value is 95.2 g N Mg^{-1}) are at the high end of the range that has been
528 observed by field studies (Fassbinder et al., 2013; Grant et al., 1999, 2006, 2008, 2016; Hamrani et al., 2020; Venterea et al.,
529 2011). Some IMVs with high feature importance scores (e.g., O_2 flux, N_2 flux) or at different depths (e.g., soil NO_3^- at 5 cm
530 depth, VWC at 5 cm depth), and data out of growing seasons are not included. The direct consequences are that some important
531 processes cannot be well represented by the current KGML-ag (e.g., O_2 demand and N availability for nitrification and
532 denitrification). Further improvement of KGML should consider three categories of data: target variable N_2O flux, IMVs and
533 basic inputs (Fig. 1a). For N_2O flux observation, we lack sub-hourly to sub-daily observations to capture the hot moment of
534 emission during 0-30 days after N fertilizer applications. Besides, the non-growing season can provide 35-65% of the annual
535 direct N_2O emissions from seasonally frozen croplands and lead to a 17–28 % underestimate of the global agricultural N_2O
536 budget if ignoring its contribution (Wagner-Riddle et al., 2017), but we can barely find observations from non-growing seasons.
537 For IMVs, we found oxygen demand indicator (e.g., O_2 concentration or flux, CO_2 flux, CH_4 flux), N mass balance related
538 variables (e.g., N_2 flux, soil NO_3^-, soil NH_4^+, N leaching) and soil water and temperature, can be used to better constrain the
539 processes and therefore improve the KGML performance. Rohe et al. (2021) also indicated the importance of O_2, CO_2 and N_2
540 soil fluxes for N_2O predictions. In addition, the layerwise soil observations (e.g., soil NO_3^-, soil VWC) at 0-30 cm depth can
541 be used to significantly improve the KGML model quality, according to our feature importance analysis (Fig. S2a). Moreover,
542 continuous monitoring on these variables during the whole year is preferred rather than only during the growing season, since
543 N_2O flux is largely influenced by previous states. To apply the KGML-ag to large scale, other observational data including
544 basic inputs of soil/crop properties (e.g., soil bulk density, pH, crop type), management information (e.g., fertilizer, irrigation,
545 tillage) and weather forcings along with N_2O flux observations are critical for fine-tuning and validating the developed KGML-
546 ag and therefore explicitly simulating the N_2O or IMVs dynamics under specific conditions. Recent advances in remote sensing
547 and machine learning have enabled estimating these variables with high-resolution at a large scale (Peng et al., 2020)

548

Second, the physical/chemical constraints can be more comprehensive in KGML-ag models. Although current KGML-ag models are well-initialized with *ecosys* synthetic data and constrained by causal relations of processes with hierarchical structure, the predicted N_2O flux and IMVs can still violate some basic physical rules like mass balance. As we discussed in Sec. 4.2, it will be challenging to add physical rules like mass balance equation for N in a complicated agriculture ecosystem due to data limitations such as missing observations on certain key variables. Using inequalities instead of equations for mass balance may be one alternative solution. For example, we could use ReLU to add in a limitation for N mass balance residues which are calculated from known terms not larger than an empirical static value. Besides, better understanding of processes in the N cycle from fieldworks and lab experiments can also help us design new constraints. This limitation is also partially related to the data limitation and can be overcomed by involving more complete N_2O data to introduce more powerful constraints to KGML-ag.

Third, the KGML-ag currently are suffering from dealing with physical/chemical boundary transitions. Boundary transitions are common in the real world, such as phase change, volume solubility, and soil porosity etc. A detailed PB model generally coded plenty of "if/else/switch" statements inside to deal with the boundaries. But KGML-ag models based on the GRU are better at capturing continuous changes, rather than discrete changes. One solution is to include data with boundary information. In this study, involving IMVs like O_2, CO_2 and N_2, which already have boundary information like water freezing point, N pool volumes and other complicated boundaries related to soil/crop properties, can significantly improve the model performance. The data with boundary information could be continuous observation or estimated value from existing data. By using initial values to predict IMVs, KGML-ag in this study can partially solve the boundary transition problem when observation data is limited. Another solution is designing new structures of KGML-ag, such as combining ReLU function or including CNN model which are robust for discrete situations to the RNN models, or designing new constraints to limit the model working within the thresholds.

Finally, at the current stage we can not claim to have completely opened the black box of KGML-ag, but this framework is a significant step towards this goal. For example, some ideas implemented in our study, such as using pretraining to transfer knowledge from a PB model to a ML model, incorporating causal relations by hierarchical structure, predicting IMVs for tracking middle changes and using initial values as input to reduce data demand, would shed light on the future KGML-ag framework improvement. Besides, we acknowledge the importance of further testing the KGML-ag over completely independent datasets, but results presented in this manuscript are sufficient to justify the power of KGML as a framework. The mesocosm experiment data we used in this study has provided a comprehensive set of inputs and intermediate variables in addition to the output of N_2O fluxes, thus serving as a unique testbed. We expect to further validate and refine our KGML-ag model once more gold standard data of N_2O fluxes along with other relevant inputs and intermediate variables become publicly available. Moreover, incorporating more and more domain knowledge into KGML-ag will be possible for further improvement, but we don't think KGML-ag will become inefficient as it becomes more like the PB model. In fact, to efficiently emulate

components of PB models has been proposed as a research frontier in hybrid modeling for earth system science (Reichstein et al., 2019; Irrgang et al., 2021), with latest advances occurring in weather forecasts (Bauer et al., 2021). By using a hybrid model, computationally inefficient components of PB can be identified one by one, and be replaced with more efficient ML-based surrogates to eventually obtain the most efficient model. Further KGML-ag model development will also need to balance efficiency, accuracy and interpretability.

5 Conclusions

In this study, two KGML-ag models have been developed, validated, and tested for agricultural soil N_2O flux prediction using synthetic data generated by the PB model *ecosys* and observational data from a mesocosm facility. The results show that KGML-ag models can outperform PB and pure ML models in N_2O prediction in not only magnitude (KGML-ag1 $r^2 = 0.81$ vs best ML model GRU $r^2 = 0.78$) but also dynamics (KGML-ag1 accuracy minus GRU accuracy, slope $\Delta r^2 = 0.06$ and curvature $\Delta r^2 = 0.08$). KGML-ag can also defeat the PB model *ecosys* in efficiency by completing *ecosys*'s half-hour job within a few seconds. Compared to ML models, KGML-ag models can better represent complex dynamics and high peaks of N_2O flux. Moreover, with IMV predictions and hierarchical structures, KGML-ag models can provide biogeophysical/chemical information about key processes controlling N_2O fluxes, which will be useful for interpretable forecasting and developing mitigation strategies. Data demand for the KGML-ag models is significantly reduced due to involving IMV initial values and pretrain processes with synthetic data. This study demonstrated that the potential of KGML-ag application in the complex agriculture ecosystem is high and illustrates possible pathways of KGML-ag development for similar tasks. Further improvement of our KGML-ag models can involve general principles to further constrain the predictions through loss functions or architectures, but call for more detailed, high temporal resolution N_2O observation data from field measurements.

Code and Data Availability

The code and data used in this study can be found at https://doi.org/10.5281/zenodo.5504533.

Author contributions

LL and ZJ conceived the study. WZ and YY conducted *ecosys* simulations and provided synthetic data. LL and SX processed the data and developed the KGML-ag model. LL, SX and SW carried the experiments out with supervisions from ZJ, JT, KG, and VK. TJG, MDE, ALF and LTM shared mesocosm observations and interpreted the data. LL wrote the first draft of the manuscript with further editing from TK on figures and tables. ZJ, SX, JT, KG, XJ, BP, YY, WZ and VK further edited the manuscript.

610   **Competing interests**

611   The authors declare that they have no conflict of interest.

612   **References**

613   Barton, L., Wolf, B., Rowlings, D., Scheer, C., Kiese, R., Grace, P., ... & Butterbach-Bahl, K.: Sampling frequency affects
614   estimates of annual nitrous oxide fluxes, Scientific reports, 5(1), 1-9, 2015.

615   Bauer, P., Dueben, P. D., Hoefler, T., Quintino, T., Schulthess, T. C., & Wedi, N. P.: The digital revolution of Earth-system
616   science. Nature Computational Science, 1(2), 104-113, 2021.

617   Beucler, T., Pritchard, M., Rasp, S., Ott, J., Baldi, P., & Gentine, P.: Enforcing analytic constraints in neural networks
618   emulating physical systems, Physical Review Letters, 126(9), 098302, 2021.

619   Beucler, T., Rasp, S., Pritchard, M., & Gentine, P.: Achieving conservation of energy in neural network emulators for climate
620   modeling, arXiv preprint arXiv:1906.06622, 2019.

621   Butterbach-Bahl, K., Baggs, E. M., Dannenmann, M., Kiese, R., & Zechmeister-Boltenstern, S.: Nitrous oxide emissions from
622   soils: how well do we understand the processes and their controls? Philosophical Transactions of the Royal Society B:
623   Biological Sciences, 368(1621), 20130122, 2013.

624   Cho, K., Van Merriënboer, B., Bahdanau, D., & Bengio, Y.: On the properties of neural machine translation: Encoder-decoder
625   approaches, arXiv preprint arXiv:1409.1259, 2014.

626   Chung, Junyoung, Caglar Gulcehre, KyungHyun Cho, and Yoshua Bengio.: Empirical evaluation of gated recurrent neural
627   networks on sequence modeling, arXiv preprint arXiv:1412.3555, 2014.

628   Daw, A., Thomas, R. Q., Carey, C. C., Read, J. S., Appling, A. P., & Karpatne, A.: Physics-guided architecture (pga) of neural
629   networks for quantifying uncertainty in lake temperature modeling, In Proceedings of the 2020 siam international conference
630   on data mining (pp. 532-540), Society for Industrial and Applied Mathematics, 2020.

631   Del Grosso, S. J., Parton, W. J., Mosier, A. R., Ojima, D. S., Kulmala, A. E., & Phongpan, S.: General model for N_2O and N2
632   gas emissions from soils due to dentrification, Global biogeochemical cycles, 14(4), 1045-1060, 2020.

633   Fassbinder, J. J, Schultz, N. M, Baker, J. M, & Griffis, T. J.: Automated, Low-Power Chamber System for Measuring Nitrous
634   Oxide Emissions, Journal of environmental quality, 42, 606. doi: 10.2134/jeq2012.0283, 2013.

635   Fassbinder, J. J., Griffis, T. J., & Baker, J. M.: Evaluation of carbon isotope flux partitioning theory under simplified and
636   controlled environmental conditions, Agricultural and forest meteorology, 153, 154-164, 2012.

637   Forster, P., Storelvmo, T., Armour, K. , Collins, W., … & Zhang, H.: The Earth's Energy Budget, Climate Feedbacks, and
638   Climate Sensitivity. In: Climate Change 2021: The Physical Science Basis. Contribution of Working Group I to the Sixth
639   Assessment Report of the Intergovernmental Panel on Climate Change, Cambridge University Press. In Press, 2021.

640   Gilhespy, S. L., Anthony, S., Cardenas, L., Chadwick, D., del Prado, A., Li, C., ... & Yeluripati, J. B.: First 20 years of DNDC
641   (DeNitrification DeComposition): model evolution, Ecological modelling, 292, 51-62, 2014.

Grant, R. F.: Modeling Carbon and Nitrogen Dynamics for Soil Management, (Boca Raton, FL: CRC Press) A review of the Canadian ecosystem model ecosys 173–264, 2021.

Grant, R. F., & Pattey, E.: Mathematical modeling of nitrous oxide emissions from an agricultural field during spring thaw. Global Biogeochemical Cycles, 13(2), 679-694, 1999.

Grant, R. F., & Pattey, E.: Modelling variability in N_2O emissions from fertilized agricultural fields, Soil Biology and Biochemistry, 35(2), 225-243, 2003.

Grant, R. F., & Pattey, E.: Temperature sensitivity of N_2O emissions from fertilized agricultural soils: Mathematical modeling in ecosys. Global biogeochemical cycles, 22(4), 2008.

Grant, R. F., Neftel, A., & Calanca, P.: Ecological controls on N_2O emission in surface litter and near-surface soil of a managed grassland: modelling and measurements, Biogeosciences, 13(12), 3549-3571, 2016.

Grant, R. F., Pattey, E., Goddard, T. W., Kryzanowski, L. M., & Puurveen, H.: Modeling the effects of fertilizer application rate on nitrous oxide emissions, Soil Science Society of America Journal, 70(1), 235-248, 2006.

Hamrani, A., Akbarzadeh, A., & Madramootoo, C. A.: Machine learning for predicting greenhouse gas emissions from agricultural soils, Science of The Total Environment, 741, 140338, 2020.

Hanson, P. C., Stillman, A. B., Jia, X., Karpatne, A., Dugan, H. A., Carey, C. C., ... & Kumar, V.: Predicting lake surface water phosphorus dynamics using process-guided machine learning, Ecological Modelling, 430, 109136, 2020.

Holzworth, D. P., Huth, N. I., deVoil, P. G., Zurcher, E. J., Herrmann, N. I., McLean, G., ... & Keating, B. A.: APSIM–evolution towards a new generation of agricultural systems simulation, Environmental Modelling & Software, 62, 327-350, 2014.

Irrgang, C., Boers, N., Sonnewald, M., Barnes, E. A., Kadow, C., Staneva, J., & Saynisch-Wagner, J.: Towards neural Earth system modelling by integrating artificial intelligence in Earth system science. Nature Machine Intelligence, 3(8), 667-674, 2021.

Jia, X., Willard, J., Karpatne, A., Read, J. S., Zwart, J. A., Steinbach, M., & Kumar, V.: Physics-guided machine learning for scientific discovery: An application in simulating lake temperature profiles, ACM/IMS Transactions on Data Science, 2(3), 1-26, 2021.

Jia, X., Willard, J., Karpatne, A., Read, J., Zwart, J., Steinbach, M., & Kumar, V.: Physics guided RNNs for modeling dynamical systems: A case study in simulating lake temperature profiles, In Proceedings of the 2019 SIAM International Conference on Data Mining (pp. 558-566), Society for Industrial and Applied Mathematics, 2019.

Karpatne, A., Atluri, G., Faghmous, J. H., Steinbach, M., Banerjee, A., Ganguly, A., ... & Kumar, V.: Theory-guided data science: A new paradigm for scientific discovery from data, IEEE Transactions on knowledge and data engineering, 29(10), 2318-2331, 2017.

Keating, B. A., Carberry, P. S., Hammer, G. L., Probert, M. E., Robertson, M. J., Holzworth, D., ... & Smith, C. J.: An overview of APSIM, a model designed for farming systems simulation, European journal of agronomy, 18(3-4), 267-288, 2003.

Khandelwal, A., Xu, S., Li, X., Jia, X., Stienbach, M., Duffy, C., ... & Kumar, V., Physics guided machine learning methods for hydrology, arXiv preprint arXiv:2012.02854, 2020.

Kim, T., Jin, Z., Smith, T., Liu, L., Yang, Y., Yang, Y., ... & Zhou, W.: Quantifying nitrogen loss hotspots and mitigation potential for individual fields in the US Corn Belt with a metamodeling approach, Environmental Research Letters, 2021.

Kraft, B., Jung, M., Körner, M., Koirala, S., & Reichstein, M.: Towards hybrid modeling of the global hydrological cycle, Hydrology and Earth System Sciences Discussions, 1-40, 2021.

Meyer, D., Nagler, T., & Hogan, R. J.: Copula-based synthetic data augmentation for machine-learning emulators. Geoscientific Model Development, 14(8), 5205-5215, 2021.

Miller, L. T. , Griffis, T. J., Erickson, M. D., Turner, P. A., Deventer, M. J., Chen, Z., Yu, Z., Venterea, R.T., Baker, J. M., and Frie, A. L.: Response of nitrous oxide emissions to future changes in precipitation and individual rain events, Journal of Environmental Quality, In review, 2021

Miller, L. T., Assessing Agricultural Nitrous Oxide Emissions and Hot Moments Using Mesocosm Simulations, (Master Thesis, University of Minnesota) Retrieved from the University of Minnesota Digital Conservancy, https://hdl.handle.net/11299/219276, 2021

Necpálová, M., Anex, R. P., Fienen, M. N., Del Grosso, S. J., Castellano, M. J., Sawyer, J. E., ... & Barker, D. W.: Understanding the DayCent model: Calibration, sensitivity, and identifiability through inverse modeling, Environmental Modelling & Software, 66, 110-130, 2015.

Oord, A. V. D., Dieleman, S., Zen, H., Simonyan, K., Vinyals, O., Graves, A., ... & Kavukcuoglu, K.: Wavenet: A generative model for raw audio, arXiv preprint arXiv:1609.03499, 2016.

Pachauri, R. K., Allen, M. R., Barros, V. R., Broome, J., Cramer, W., Christ, R., ... & van Ypserle, J. P.: Climate change 2014: synthesis report. Contribution of Working Groups I, II and III to the fifth assessment report of the Intergovernmental Panel on Climate Change (p. 151). Ipcc, 2014.

Read, J. S., Jia, X., Willard, J., Appling, A. P., Zwart, J. A., Oliver, S. K., ... & Kumar, V.: Process-guided deep learning predictions of lake water temperature, Water Resources Research, 55(11), 9173-9190, 2019.

Peng, B., Guan, K., Tang, J., Ainsworth, E. A., Asseng, S., Bernacchi, C. J., ... & Zhou, W.: Towards a multiscale crop modelling framework for climate change adaptation assessment, Nature plants, 6(4), 338-348, 2020.

Reichstein, M., Camps-Valls, G., Stevens, B., Jung, M., Denzler, J., & Carvalhais, N.: Deep learning and process understanding for data-driven Earth system science. Nature, 566(7743), 195-204, 2019.

Robertson, M., BenDor, T. K., Lave, R., Riggsbee, A., Ruhl, J. B., & Doyle, M.: Stacking ecosystem services, Frontiers in Ecology and the Environment, 12(3), 186-193, 2014.

Rohe, L., Apelt, B., Vogel, H. J., Well, R., Wu, G. M., & Schlüter, S.: Denitrification in soil as a function of oxygen availability at the microscale, Biogeosciences, 18(3), 1185-1201, 2021.

Saha, D., Basso, B., & Robertson, G. P.: Machine learning improves predictions of agricultural nitrous oxide (N_2O) emissions from intensively managed cropping systems, Environmental Research Letters, 16(2), 024004, 2021.

709 Solazzo, E., Crippa, M., Guizzardi, D., Muntean, M., Choulga, M., & Janssens-Maenhout, G.: Uncertainties in the Emissions
710 Database for Global Atmospheric Research (EDGAR) emission inventory of greenhouse gases, Atmospheric Chemistry and
711 Physics, 21(7), 5655-5683, 2021.

712 Solazzo, E., Crippa, M., Guizzardi, D., Muntean, M., Choulga, M., & Janssens-Maenhout, G.: Uncertainties in the Emissions
713 Database for Global Atmospheric Research (EDGAR) emission inventory of greenhouse gases, Atmospheric Chemistry and
714 Physics, 21(7), 5655-5683, 2021.

715 Syakila, A., & Kroeze, C.: The global nitrous oxide budget revisited, Greenhouse gas measurement and management, 1(1),
716 17-26, 2011.

717 Thompson, R. L., Lassaletta, L., Patra, P. K., Wilson, C., Wells, K. C., Gressent, A., ... & Canadell, J. G.: Acceleration of
718 global N_2O emissions seen from two decades of atmospheric inversion, Nature Climate Change, 9(12), 993-998, 2019.

719 Thornley, J. H., & France, J.: Mathematical models in agriculture: quantitative methods for the plant, animal and ecological
720 sciences, Cabi, 2007.

721 Tian, H., Xu, R., Canadell, J. G., Thompson, R. L., Winiwarter, W., Suntharalingam, P., ... & Yao, Y.: A comprehensive
722 quantification of global nitrous oxide sources and sinks, Nature, 586(7828), 248-256, 2020.

723 Venterea, R. T., Maharjan, B., & Dolan, M. S.: Fertilizer source and tillage effects on yield-scaled nitrous oxide emissions in
724 a corn cropping system. Journal of Environmental Quality, 40(5), 1521-1531, 2011.

725 Wagner-Riddle, C., Congreves, K. A., Abalos, D., Berg, A. A., Brown, S. E., Ambadan, J. T., ... & Tenuta, M.: Globally
726 important nitrous oxide emissions from croplands induced by freeze–thaw cycles, Nature Geoscience, 10(4), 279-283, 2017.

727 Willard, J., Jia, X., Xu, S., Steinbach, M., & Kumar, V.: Integrating Scientific Knowledge with Machine Learning for
728 Engineering and Environmental Systems, arXiv preprint arXiv:2003.04919, 2020.

729 Zhang, Y., & Niu, H.: The development of the DNDC plant growth sub-model and the application of DNDC in agriculture: a
730 review, Agriculture, Ecosystems & Environment, 230, 271-282, 2016.

731 Zhang, Y., Li, C., Zhou, X., & Moore III, B.: A simulation model linking crop growth and soil biogeochemistry for sustainable
732 agriculture, Ecological modelling, 151(1), 75-108, 2002.

733 Zhou, W., Guan, K., Peng, B., Tang, J., Jin, Z., Jiang, C., ... & Mezbahuddin, S.: Quantifying carbon budget, crop yields and
734 their responses to environmental variability using the ecosys model for US Midwestern agroecosystems. Agricultural and
735 Forest Meteorology, 307, 108521, 2021.
736
737
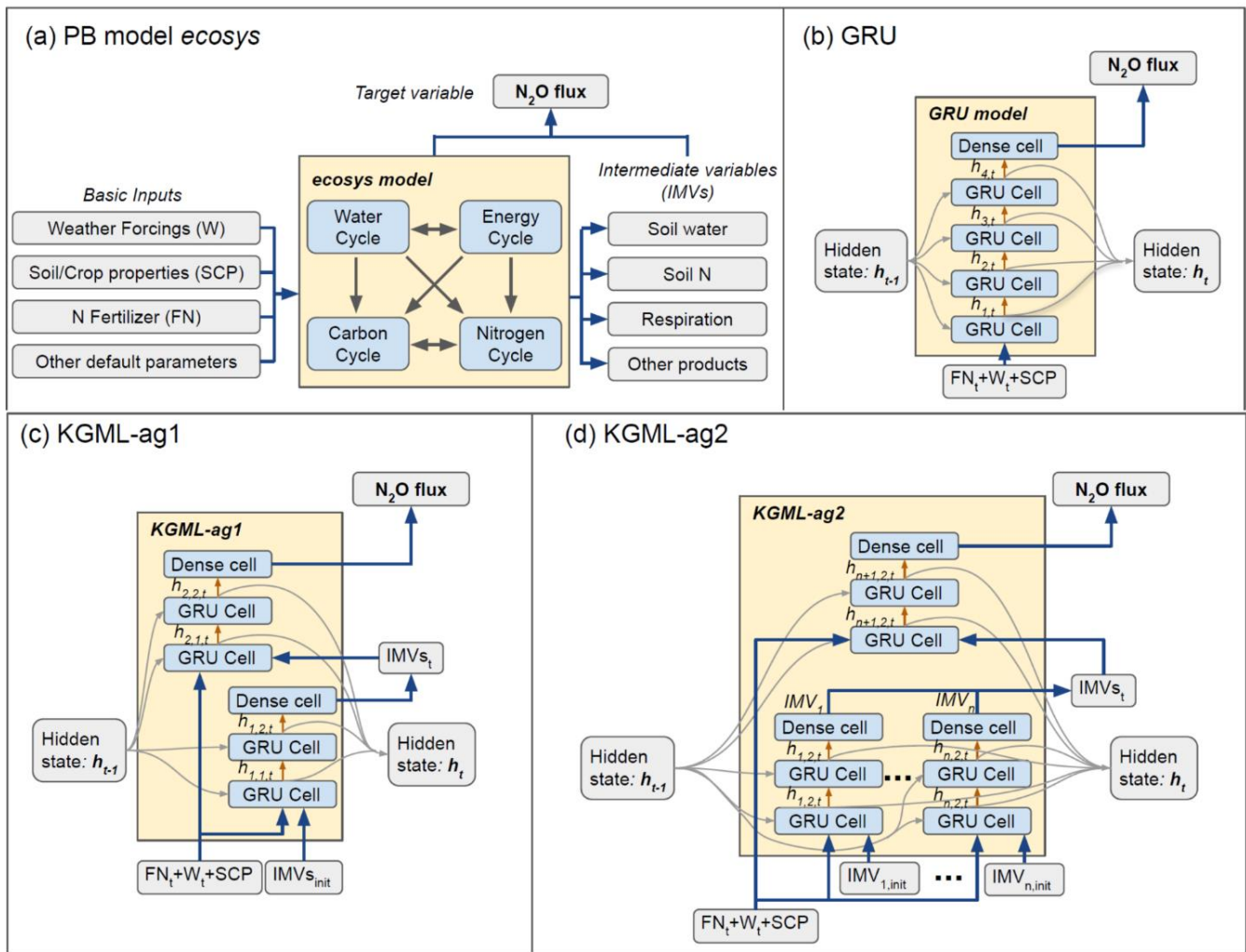
Figure 1: The model structures. a) The *ecosys* model; b) Gated recurrent unit (GRU) model; c) KGML-ag1 model with a hierarchical structure; d) KGML-ag2 model with a hierarchical structure with separated GRU modules for IMV predictions. Specifically, in our KGML model design, weather forcings (W) include temperature (TMAX, TDIF), precipitation (PRECN), radiation (RADN), humidity (HMAX and HDIF) and wind speed (WIND); soil/crop properties (SCP) include bulk density (TBKDS), sand content (TCSAND), silt content (TCSILT), pH (TPH), cation exchange capacity (TCEC), soil organic carbon (TSOC), planting day of the year (PDOY) and crop type (CROPT); IMVs include CO_2 flux, soil NO_3^- concentration, soil NH_4^+ concentration, and soil volumetric water content (VWC).

747
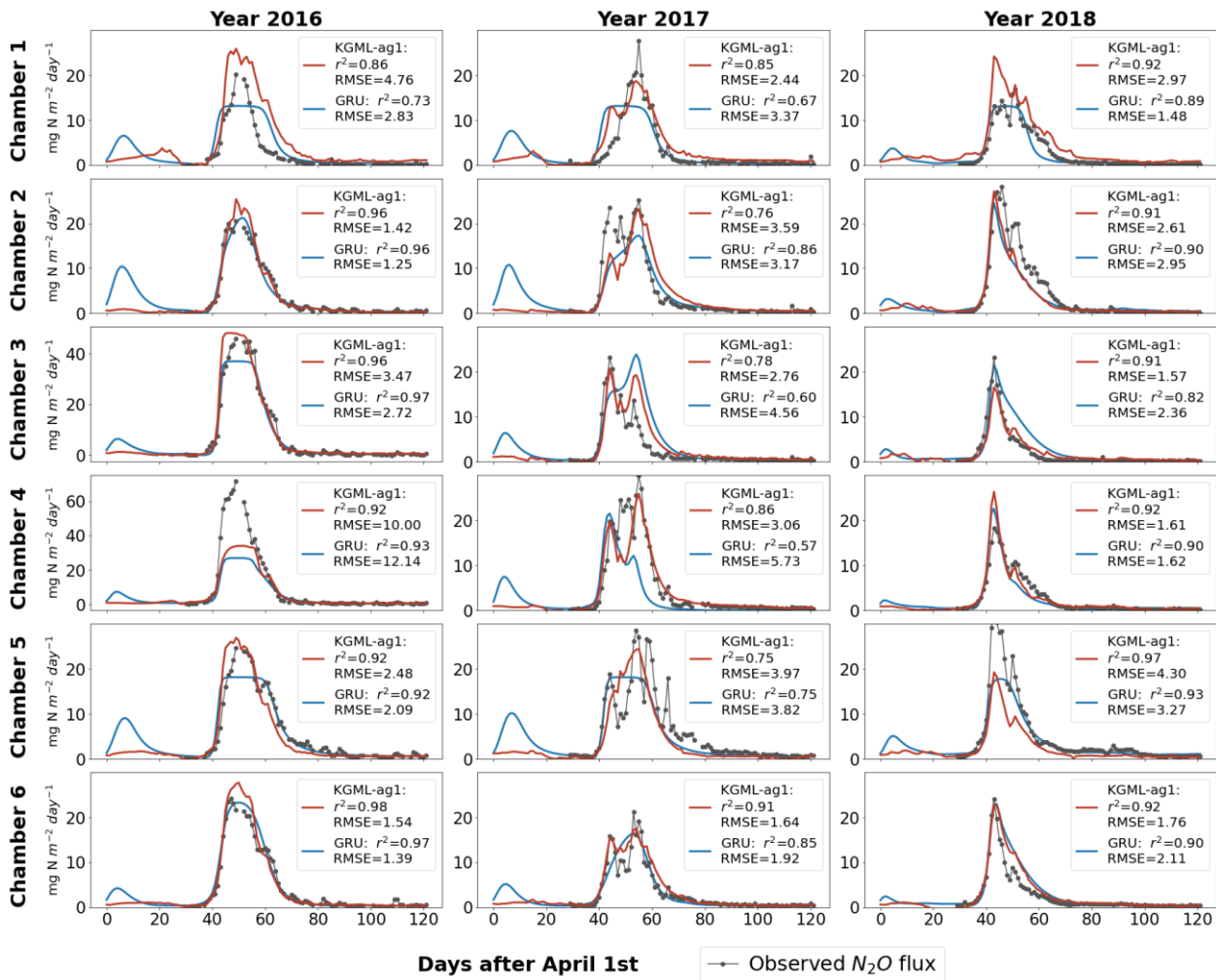
Figure 2: Leave-one-out cross validation of time series of N₂O flux (mg N m⁻² day⁻¹) predicted by the pure non-pretrained GRU
model (blue line) and KGML-ag1 model (red line). Observations are shown as black line-dots. Validation results for each chamber
were based on out-of-sample predictions by models trained by other five chambers.

751
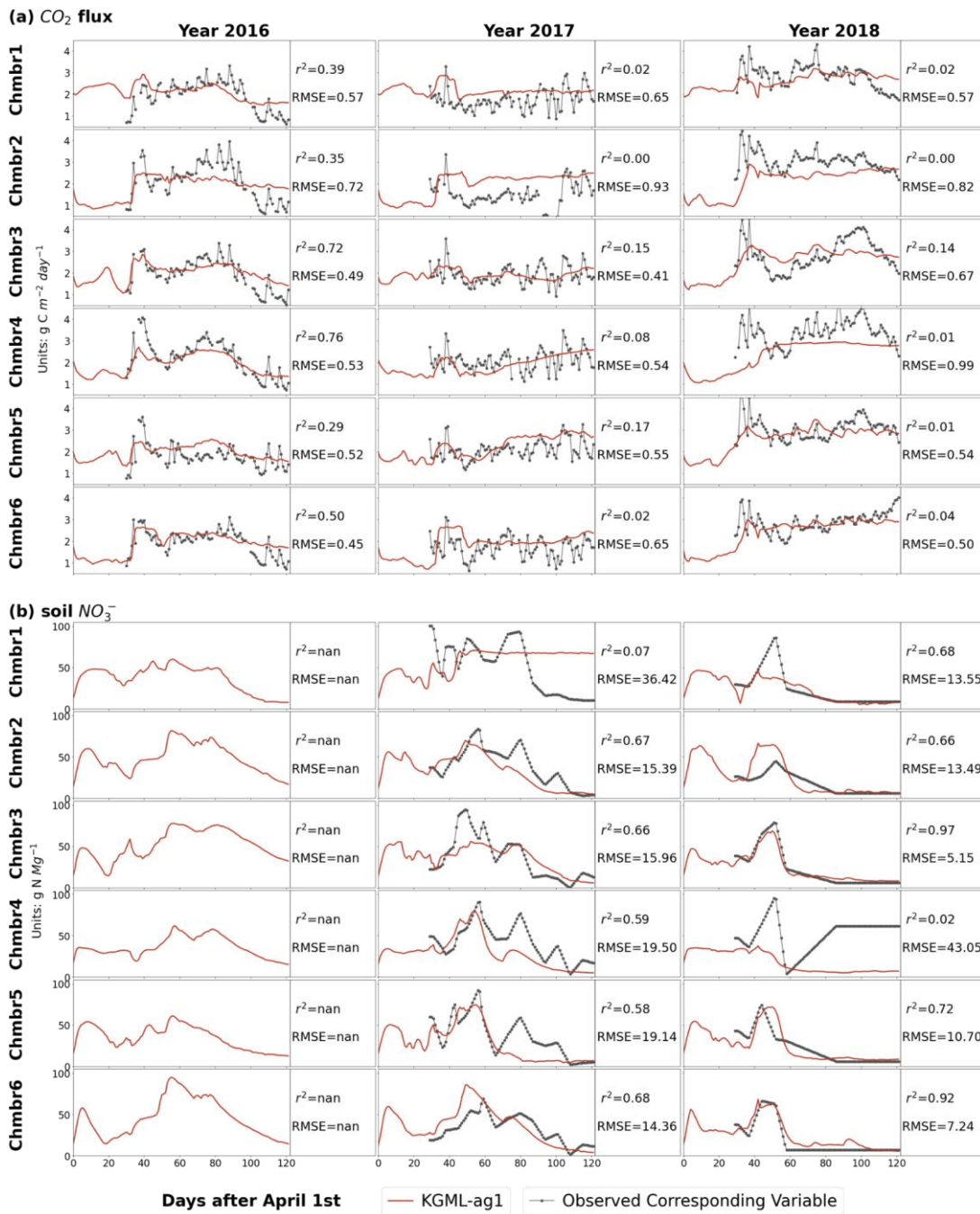
Figure 3: Leave-one-out cross validation of time series of IMVs predicted by KGML-ag1 model (red line). Observations are shown as black line-dots. Validation results for each chamber were based on out-of-sample predictions by models trained by other five chambers. Chmb is the abbreviation for chamber. r^2 and RMSE are calculated and present in each year and chamber. The CO_2 flux and soil NO_3^- concentration units are g C m^{-2} day^{-1} and g N Mg^{-1}, respectively.
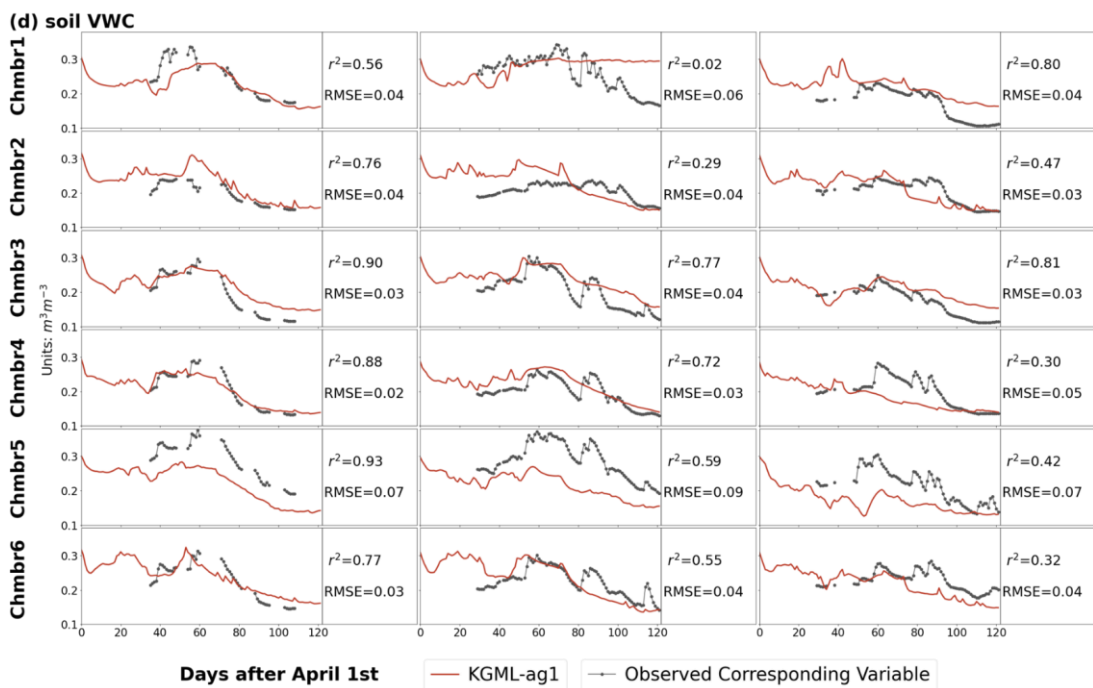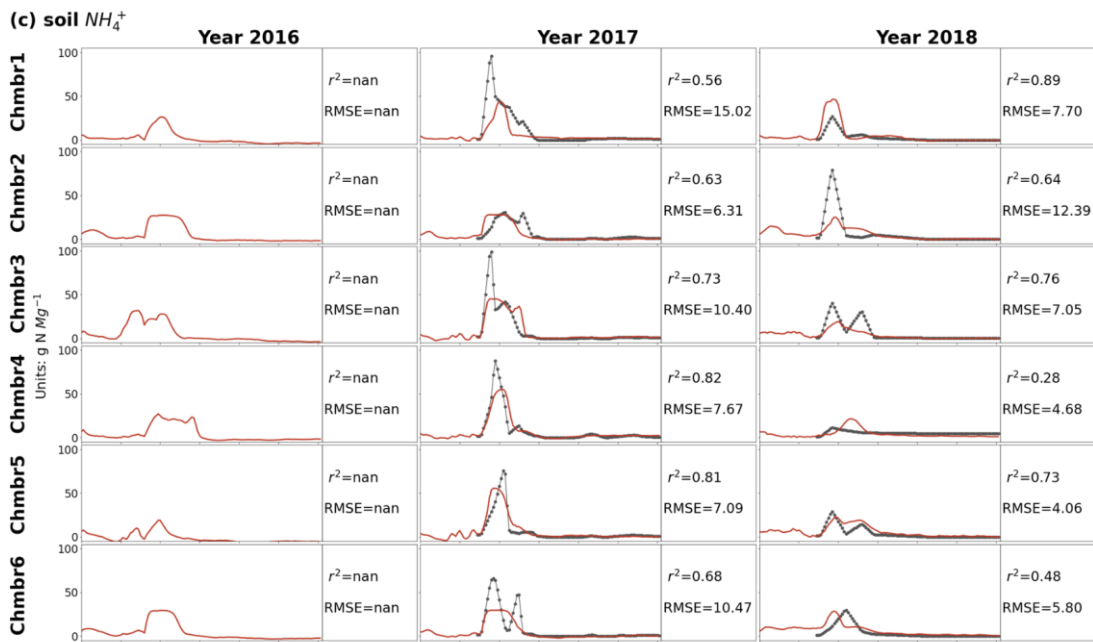
Figure 3 Contd.: Leave-one-out cross validation of time series of IMVs predicted by KGML-ag1 model (red line). Observations are shown as black line-dots. Validation results for each chamber were based on out-of-sample predictions by models trained by other five chambers.Chmb is the abbreviation for chamber. r^2 and RMSE are calculated and present in each year and chamber. The soil NH$_4^+$ concentration and soil VWC units are g N Mg^{-1} and m^3 m^{-3}, respectively.

763

764
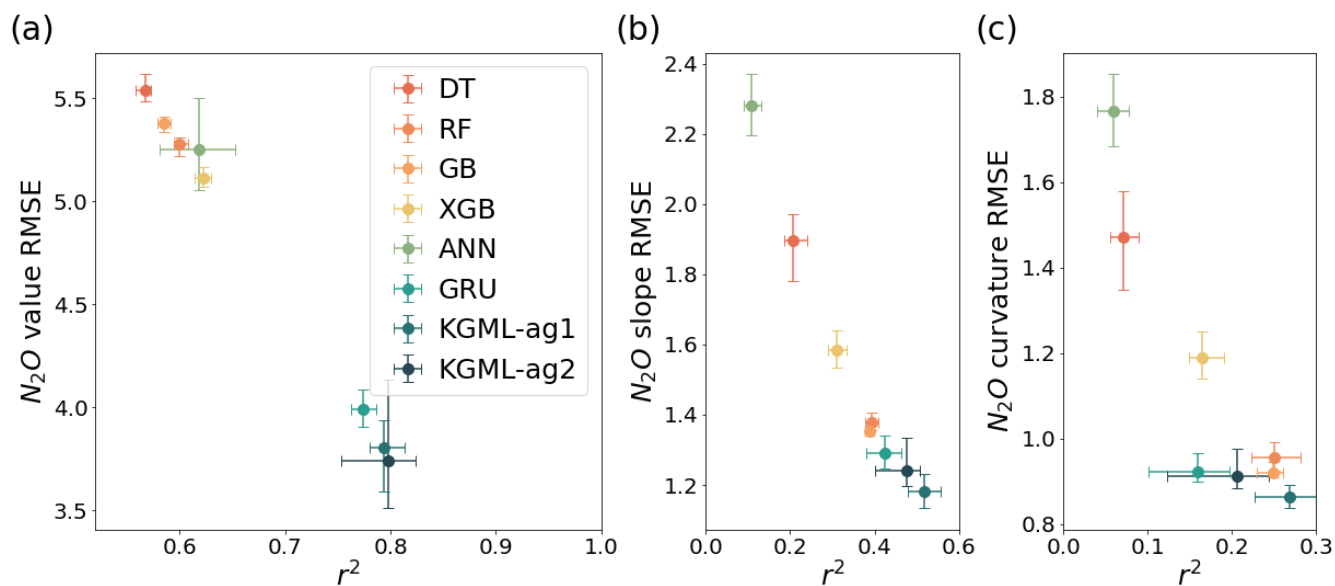
Figure 4: The comparisons of overall prediction accuracy from leave-one-out cross validation for N₂O value (a), 1st order gradient (slope, b) and 2nd order gradient (curvature, c) between four tree-based ML models (DT, RF, GB and XGB), two deep learning models (ANN and GRU) and KGML-ag models. The overall performances were calculated by comparing out-of-sample predictions (each chamber's predictions were from models trained by other five chambers) from all validated chambers with observations. Different color symbols represent the different models. The x- and y-error bars are coming from the maximum and minimum scores of ensemble experiments. The dot represents the mean score of the ensemble experiments.

771

772
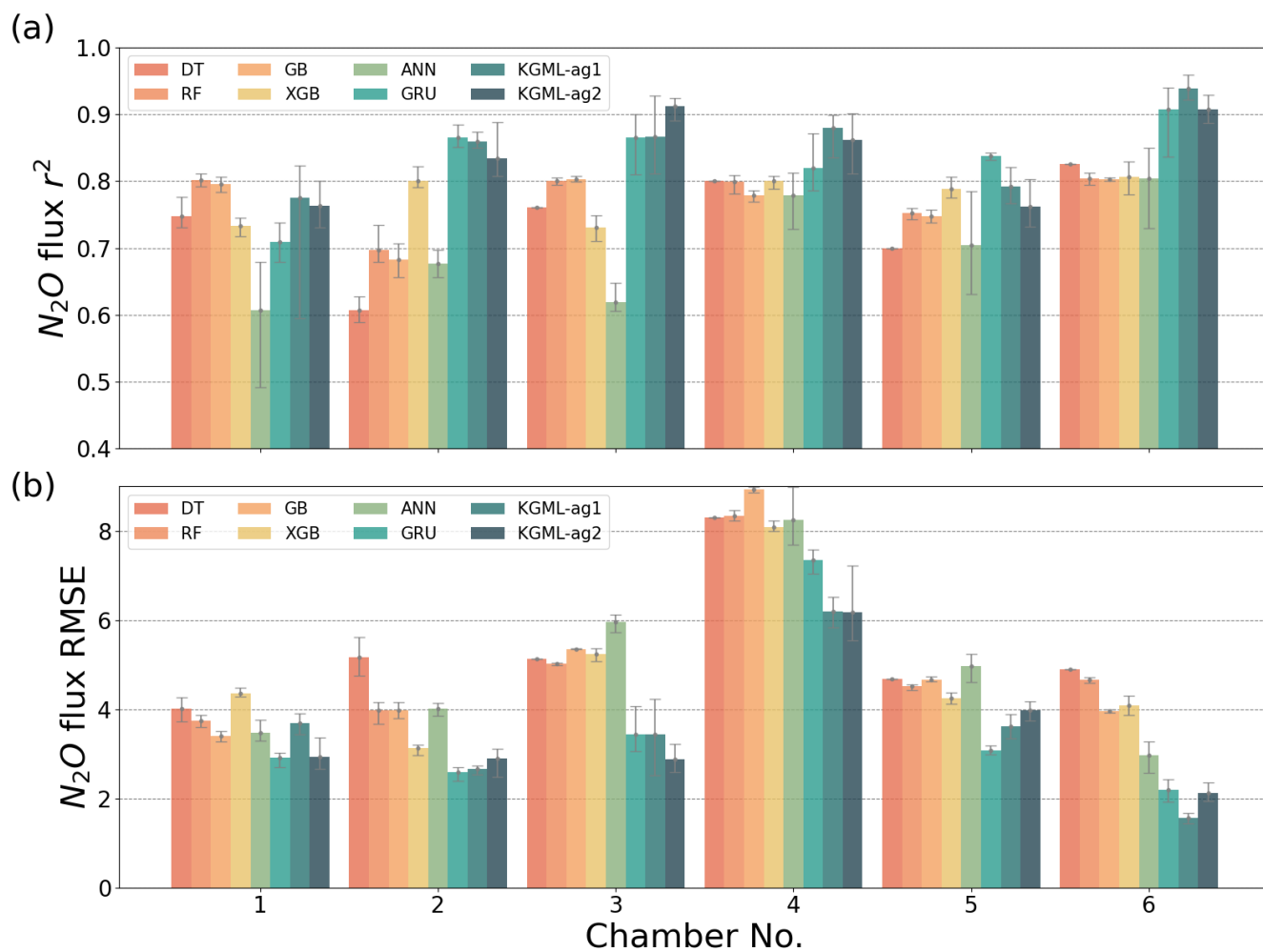
Figure 5: The comparisons of N₂O flux prediction accuracy r² (a) and (b) RMSE from leave-one-out cross validation, between four tree-based ML models (DT, RF, GB and XGB), two deep learning models (ANN and GRU) and KGML-ag models in six chambers. Validation results for each chamber were based on out-of-sample predictions by models trained by other five chambers. The gray error bars are coming from the maximum and minimum scores of ensemble experiments.

777

Table 1: Pretrain results for different model and IMV combinations using *ecosys* synthetic data. Only performances from testing data sets (synthetic data from 19 counties) were presented.

			N_2O		CO_2		NO_3^-		NH_4^+		VWC	
No.	Pretrain Model	Input Feature N	r^2	RMSE	r^2	NRMSE	r^2	NRMSE	r^2	NRMSE	r^2	NRMSE
1	GRU+76IMVs	76 IMVs+FN+7Ws+8SCP	0.98	0.54	--[a]	--	--	--	--	--	--	--
2	GRU+IMVcb1	4 IMVs+FN+7Ws+8SCP	0.92	1.15	--	--	--	--	--	--	--	--
3	GRU+IMVcb2	3 IMVs+FN+7Ws+8SCP	0.90	1.26	--	--	--	--	--	--	--	--
4	GRU	FN+7Ws+8SCP	0.89	1.37	--	--	--	--	--	--	--	--
5	KGML-ag1+IMVcb1_ini	FN+7Ws+8SCP+4IMV_ini	0.90	1.24	0.91	0.06	0.95	0.03	0.98	0.03	0.95	0.04
6	KGML-ag1+IMVcb2_ini	FN+7Ws+8SCP+3IMV_ini	0.90	1.26	--	--	0.94	0.03	0.97	0.03	0.95	0.04
7	KGML-ag2+IMVcb1_ini	FN+7Ws+8SCP+4IMV_ini	0.90	1.27	0.92	0.05	0.95	0.02	0.98	0.03	0.96	0.04
8	KGML-ag2+IMVcb2_ini	FN+7Ws+8SCP+3IMV_ini	0.91	1.19	--	--	0.95	0.00	0.99	0.02	0.95	0.04

[a]The empty slot indicates that the model does not predict that variable.

Table 2: Prediction accuracy comparisons between non-pretrained GRU model and KGML-ag1.

	No.	N_2O, KGML-ag1 minus GRU				N_2O 1st order gradient, KGML-ag1 minus GRU				N_2O 2nd order gradient, KGML-ag1 minus GRU			
		All time[b]	Day 30-80	Day 40-65	Day 45-60	All time	Day 30-80	Day 40-65	Day 45-60	All time	Day 30-80	Day 40-65	Day 45-60
	All data	0.03[c]	0.04	0.07	0.10	0.07	0.07	0.07	0.15	0.08	0.08	0.09	0.11
	Chamber1	0.07	0.10	0.20	0.13	0.18	0.18	0.19	0.14	0.08	0.09	0.09	0.02
	Chamber2	**-0.04**	**-0.05**	**-0.07**	**-0.05**	0.08	0.09	0.09	0.16	0.20	0.20	0.20	0.23
$\Delta r^{2\ a}$	**Chamber3**	0.06	0.06	0.08	0.06	0.04	0.04	0.04	0.13	**-0.01**	**-0.01**	**-0.01**	0.07
	Chamber4	0.06	0.08	0.12	0.07	0.05	0.05	0.05	0.14	0.07	0.07	0.08	0.12
	Chamber5	**-0.05**	**-0.06**	**-0.07**	**-0.03**	0.09	0.09	0.10	0.16	0.13	0.13	0.15	0.11
	Chamber6	0.03	0.04	0.08	0.17	0.14	0.14	0.15	0.22	0.12	0.13	0.14	0.23
	All data	-0.41	-0.56	-0.84	-1.19	-0.07	-0.10	-0.14	-0.20	-0.03	-0.05	-0.07	-0.08
	Chamber1	**0.80**	**1.06**	**1.21**	**1.70**	0.00	0.00	-0.02	0.00	**0.05**	**0.07**	**0.10**	**0.18**
	Chamber2	**0.08**	**0.11**	**0.07**	-0.04	-0.10	-0.13	-0.18	-0.14	-0.10	-0.14	-0.19	-0.22
$\Delta RMSE^a$	**Chamber3**	-0.71	-0.96	-1.30	-2.09	**0.03**	**0.04**	**0.07**	**-0.25**	**0.09**	**0.13**	**0.17**	**0.08**
	Chamber4	-1.68	-2.27	-3.09	-3.81	-0.11	-0.15	-0.21	-0.26	-0.05	-0.07	-0.09	-0.16
	Chamber5	**0.53**	**0.69**	**0.86**	**0.99**	-0.10	-0.14	-0.20	-0.23	-0.09	-0.12	-0.18	-0.14
	Chamber6	-0.20	-0.27	-0.37	-0.61	-0.14	-0.20	-0.29	-0.33	-0.07	-0.10	-0.15	-0.19

[a]Leave-one-out cross validation results for each chamber were based on out-of-sample predictions by models trained by other five chambers.

The "All data" performances were calculated by comparing out-of-sample predictions from all validated chambers with observations. The

difference of r^2 (Δr^2), and difference of RMSE (ΔRMSE, units are mg N m^{-2} day^{-1}, mg N m^{-2} day^{-2}, mg N m^{-2} day^{-3} for N_2O value, 1st order

gradient and 2nd order gradient, respectively) were calculated by values from KGML-ag1 minus values from GRU.

[b]Results from different time windows of different chambers during the period of April 1st-July31st (Days1-122) were detected.

 [c]None bold values mean KGML-ag1 outperforms GRU, while **bold** values mean the opposite.

789

790

791 **Table 3: Experiments for measuring GRU and KGML-ag models performance, and influence of pretraining process, training data**
792 **augmentation and IMV initial values.**

No.	Retrain Model	Experiment	N_2O		N_2O 1st order gradient		N_2O 2nd order gradient		CO_2		NO_3^-		NH_4^+		VWC	
			$r^{2\,c}$	$RMSE^c$	r^2	RMSE	r^2	RMSE	r^2	NRMSE	r^2	NRMSE	r^2	NRMSE	r^2	NRMSE
1	**GRU, baseline[a]**	**No Pretrain**	**0.78**	**4.00**	**0.45**	**1.27**	**0.20**	**0.90**	**--[b]**	**--**	**--**	**--**	**--**	**--**	**--**	**--**
2	GRU	Pretrain	0.80	3.77	0.57	1.12	0.34	0.82	--	--	--	--	--	--	--	--
3	KGML-ag1+IMVcb1_ini	Original setting	0.81	3.60	0.51	1.20	0.28	0.87	0.37	0.14	0.39	0.21	0.60	0.09	0.33	0.18
4	KGML-ag1+IMVcb2_ini	Original setting	0.80	3.71	0.49	1.22	0.21	0.91	--	--	0.37	0.22	0.53	0.10	0.33	0.19
5	KGML-ag2+IMVcb1_ini	Original setting	0.79	3.77	0.48	1.23	0.22	0.90	0.74	0.09	0.46	0.18	0.66	0.08	0.84	0.08
6	KGML-ag2+IMVcb2_ini	Original setting	0.78	3.91	0.47	1.24	0.20	0.91	--	--	0.49	0.18	0.69	0.08	0.84	0.08
7	KGML-ag1+IMVcb1_ini	No augmentation	0.80	3.73	0.49	1.22	0.22	0.90	0.38	0.14	0.38	0.21	0.61	0.09	0.37	0.17
8	KGML-ag1+IMVcb2_ini	No augmentation	0.77	4.04	0.41	1.31	0.13	0.95	--	--	0.38	0.21	0.53	0.10	0.35	0.18
9	KGML-ag2+IMVcb1_ini	No augmentation	0.76	4.06	0.45	1.27	0.16	0.95	0.69	0.10	0.21	0.25	0.60	0.09	0.80	0.09
10	KGML-ag2+IMVcb2_ini	No augmentation	0.74	4.27	0.48	1.23	0.21	0.90	--	--	0.40	0.21	0.60	0.09	0.81	0.09
11	KGML-ag1+IMVcb1_ini	Zero initial values	0.48	6.27	0.26	1.49	0.08	1.00	0.19	0.16	0.25	0.25	0.47	0.12	0.14	0.25
12	KGML-ag1+IMVcb2_ini	Zero initial values	0.49	5.94	0.31	1.41	0.13	0.95	--	--	0.31	0.25	0.38	0.13	0.24	0.25
13	KGML-ag2+IMVcb1_ini	Zero initial values	0.48	6.05	0.12	1.66	0.01	1.09	0.58	0.12	0.34	0.25	0.21	0.13	0.56	0.31
14	KGML-ag2+IMVcb2_ini	Zero initial values	0.39	6.60	0.15	1.59	0.04	1.01	--	--	0.16	0.27	0.27	0.12	0.53	0.31

793 [a]No.1-6 includes the experiments with original simulation settings as described in Sec. 2 and bold values refers to the baseline GRU
794 simulation; No.7-10 include the experiments without data augmentation during the finetuning process; And No. 11-14 includes the
795 experiments of replacing original IMV initial values with zeros.

796 [b]The empty slot indicates that the model does not predict that variable.

797 [c]The leave-one-out cross validation overall performances were calculated by comparing out-of-sample predictions (each chamber's
798 predictions were from models trained by other five chambers) from all validated chambers with observations.